



**HAL**  
open science

## Assessing methane emissions for northern peatlands in ORCHIDEE-PEAT revision 7020

Elodie Salmon, Fabrice Jegou, Bertrand Guenet, Line Jourdain, Chunjing Qiu, Vladislav Bastrikov, Christophe Guimbaud, Dan Zhu, Philippe Ciais, Philippe Peylin, et al.

► **To cite this version:**

Elodie Salmon, Fabrice Jegou, Bertrand Guenet, Line Jourdain, Chunjing Qiu, et al.. Assessing methane emissions for northern peatlands in ORCHIDEE-PEAT revision 7020. 2021. insu-03578235

**HAL Id: insu-03578235**

**<https://insu.hal.science/insu-03578235v1>**

Preprint submitted on 17 Feb 2022

**HAL** is a multi-disciplinary open access archive for the deposit and dissemination of scientific research documents, whether they are published or not. The documents may come from teaching and research institutions in France or abroad, or from public or private research centers.

L'archive ouverte pluridisciplinaire **HAL**, est destinée au dépôt et à la diffusion de documents scientifiques de niveau recherche, publiés ou non, émanant des établissements d'enseignement et de recherche français ou étrangers, des laboratoires publics ou privés.



## Assessing methane emissions for northern peatlands in ORCHIDEE-PEAT revision 7020.

Elodie Salmon<sup>1</sup>, Fabrice Jégou<sup>1</sup>, Bertrand Guenet<sup>2,3</sup>, Line Jourdain<sup>1</sup>, Chunjing Qiu<sup>2</sup>, Vladislav Bastrov<sup>4</sup>, Christophe Guimbaud<sup>1</sup>, Dan Zhu<sup>2,5</sup>, Philippe Ciais<sup>2</sup>, Philippe Peylin<sup>2</sup>, Sébastien Gogo<sup>6</sup>,  
5 Fatima Laggoun-Défarge<sup>6</sup>, Mika Aurela<sup>7</sup>, M. Sydonia Bret-Harte<sup>8</sup>, Jiquan Chen<sup>9</sup>, Bogdan H. Chojnicki<sup>10</sup>, Housen Chu<sup>11</sup>, Colin W. Edgar<sup>8</sup>, Eugenie S. Euskirchen<sup>8</sup>, Lawrence B. Flanagan<sup>12</sup>, Krzysztof Fortuniak<sup>13</sup>, David Holl<sup>14</sup>, Janina Klatt<sup>15</sup>, Olaf Kolle<sup>16</sup>, Natalia Kowalska<sup>17</sup>, Lars Kutzbach<sup>14</sup>, Annalea Lohila<sup>7</sup>, Lutz Merbold<sup>18</sup>, Włodzimierz Pawlak<sup>13</sup>, Torsten Sachs<sup>19</sup>, Klaudia Ziemblińska<sup>20</sup>.

10

<sup>1</sup>Laboratoire de Physique et Chimie de l'Environnement et de l'Espace, LPC2E, UMR 7328, Université d'Orléans, CNRS, CNES, 45071 Orléans cedex 2, France.

<sup>2</sup>Laboratoire des Sciences du Climat et de l'Environnement, UMR8212, CEA-CNRS-UVSQ F- 91191 Gif sur Yvette, France.

15 <sup>3</sup> Laboratoire de Géologie de l'ENS, IPSL, CNRS, PSL Research University, Laboratoire de Géologie de l'ENS, 24 rue Lhomond, 75231 Paris cedex 05, France.

<sup>4</sup>Science Partners, 75010 Paris, France.

<sup>5</sup> Sino-French Institute for Earth System Science, College of Urban and Environmental Sciences, Peking University, Beijing, China.

20 <sup>6</sup> Institut des Sciences de la Terre d'Orléans, Université d'Orléans, CNRS, BRGM, UMR 7327, 45071 Orléans, France.

<sup>7</sup> Finnish Meteorological Institute, Climate Research Programme, Helsinki, Finland

<sup>8</sup> Institute of Arctic Biology, University of Alaska Fairbanks, Fairbanks, AK, USA.

<sup>9</sup> Landscape Ecology & Ecosystem Science (LEES) Lab, Department of Geography, Environment, and Spatial Sciences, & Center for Global Change and Earth Observations, Michigan State University, East Lansing, MI 48823

25 <sup>10</sup> Laboratory of Bioclimatology, Department of Ecology and Environmental Protection, Faculty of Environmental Engineering and Mechanical Engineering, Poznan University of Life Sciences, Piątkowska 94, 60-649 Poznań, Poland

<sup>11</sup> Climate and Ecosystem Sciences Division, Lawrence Berkeley National Lab, USA, 1 Cyclotron Rd, Berkeley, CA 94720

<sup>12</sup> Department of Biological Sciences, University of Lethbridge, 4401 University Drive, Lethbridge, Alberta, Canada T1K 3M4

30 <sup>13</sup> Department of Meteorology and Climatology, Faculty of Geographical Sciences, University of Lodz, Lodz, Poland

<sup>14</sup> Institute of Soil Science, Center for Earth System Research and Sustainability (CEN), Universität Hamburg, Hamburg, Germany

<sup>15</sup> Institute of Ecology and Landscape, Chair of Vegetation Ecology, University of Applied Sciences Weihenstephan-Triesdorf, Am Hofgarten 1, 85354 Freising, Germany

35 <sup>16</sup> Field Experiments and Instrumentation, Max-Planck-Institute for Biogeochemistry, Hans-Knoell-Strasse 10, D-07745 Jena, Germany

<sup>17</sup> Department of Matter and Energy Fluxes, Global Change Research Institute, Czech Academy of Sciences, Bělidla 986/4a, 603 00 Brno, Czech Republic.

<sup>18</sup> Department Agroecology and Environment, Agroscope, Reckenholzstrasse 191, 8046 Zurich, Switzerland

40 <sup>19</sup> GFZ German Research Centre for Geosciences, Telegrafenberg, Potsdam, Germany

<sup>20</sup> Laboratory of Meteorology, Department of Construction and Geoenvironment, Faculty of Environmental Engineering and Mechanical Engineering, Poznan University of Life Sciences, Piątkowska 94, 60-649 Poznań, Poland.



45 *Correspondence to:* Elodie Salmon ([elodie.salmon@cnrs-orleans.fr](mailto:elodie.salmon@cnrs-orleans.fr)), Fabrice Jegou ([fabrice.jegou@cnrs-orleans.fr](mailto:fabrice.jegou@cnrs-orleans.fr))

**Abstract.** In the global methane budget, the largest natural source is attributed to wetlands that encompass all ecosystems composed of waterlogged or inundated ground, capable of methane production. Among them, northern peatlands that store large amounts of soil organic carbon have been functioning, since the end of the last glaciation period, as long-term sources of methane (CH<sub>4</sub>) and are one of the most significant methane sources among wetlands. To reduce global methane budget uncertainties, it is of significance to understand processes driving methane production and fluxes in northern peatlands. A methane model that features methane production and transport by plants, ebullition process and diffusion in soil, oxidation to CO<sub>2</sub> and CH<sub>4</sub> fluxes to the atmosphere has been embedded in the ORCHIDEE-PEAT land surface model which includes an explicit representation of northern peatlands. This model, ORCHIDEE-PCH4 was calibrated and evaluated on 14 peatland sites distributed on both Eurasian and American continents in the northern boreal and temperate regions. Data assimilation approaches were employed to optimized parameters at each site and at all sites simultaneously. Results show that, in ORCHIDEE-PCH4, methanogenesis is sensitive to temperature and substrate availability over the top 75 cm of soil depth. Methane emissions estimated using single site optimization (SSO) of model parameters are underestimated by 9 g CH<sub>4</sub> m<sup>-2</sup> year<sup>-1</sup> on average (i.e. 50% higher than the site average of yearly methane emissions). While using the multi-sites optimization (MSO), methane emissions are overestimated by 5 g CH<sub>4</sub> m<sup>-2</sup> year<sup>-1</sup> on average across all investigated sites (i.e. 37% lower than the site average of yearly methane emissions).

## 1 Introduction

Atmospheric methane level estimated from ice cores analysis (Etheridge et al., 1998) and in situ measurements (Blake et al., 1982; Dlugokencky, 2019; Prinn et al., 2018) have nearly tripled since the pre-industrial equilibrium value i.e., from 680 ppb to reach a value of 1892 ppb in December 2020 (Dlugokencky, 2021; Saunio et al., 2020). This increase is consistent with the world population increase and the industrialization, for instance the increase of fossil fuel extraction and use, of organic waste generation, and of livestock numbers (Raynaud et al., 2003).

Methane is the second most important anthropogenic greenhouse gas after CO<sub>2</sub>, and accounts for about 23% of the cumulative total radiative forcing (Etminan et al., 2016). In the troposphere methane is an ozone precursor and, in the stratosphere, methane interacts with hydroxyl radicals and carbon monoxide to produce water vapor. About 90% of CH<sub>4</sub> is oxidized by hydroxyl radical in the troposphere (Smith et al., 2003) and reactions with chlorine in the stratosphere or in the marine boundary layer (Allan et al., 2007; Thornton et al., 2010) leading to a residence time of about 9 years (Prather et al., 2012). At the continental surface, 5 to 10% of all methane sources are removed from the atmosphere by diffusion in soils and oxidation by soil microorganisms (Krüger et al., 2002; Prather et al., 1995; Smith et al., 2003, 1991; Tokida et al., 2007a, 2007b). Among natural sources, natural wetlands are the largest contributor and the most uncertain one in the global budget (Kirschke et al., 2013; Saunio et al., 2016). They contribute to 25 – 30% of total methane emissions estimated by Saunio et



al., (2020) and encompass anaerobic ecosystems composed of waterlogged or inundated ground that are capable of methane production which include peatlands, mineral soil wetlands and floodplains. Peatlands are of particular interests considering that peat is composed of organic detritus and has an average carbon content of 52% dry mass (Gorham, 1991). Therefore, 80 peatlands are large soil organic carbon reservoirs that could be functioning as a source of CH<sub>4</sub> and source or a sink of CO<sub>2</sub> to the atmosphere. They cover around 3% of surface continental lands but store around one third of the global soil carbon (Gorham, 1991). They are located in boreal and sub-arctic regions (80%, Strack et al., 2008) and some smaller areas are found in temperate and tropical regions (10-12%). Since the end of the last glaciation period (around 16500 years), northern peatlands have been functioning as long-term carbon sinks. This storage results from a delicate balance between carbon 85 inputs (CO<sub>2</sub> absorbed by photosynthesis) and carbon outputs (CO<sub>2</sub> and CH<sub>4</sub> production, dissolved and particulate carbon). Therefore, in these ecosystems, processes controlling methane production, fluxes between the land surface and the atmosphere and feedback on climate are intimately connected.

The major pathway of methane production is via microbial processes which is limited by the availability of substrates (polymeric and monomeric compounds derived from carbohydrates, fatty acids, amino-acids, acetate and 90 hydrogen; (Blodau, 2002; Le Mer and Roger, 2001), the low oxygen content that is directly correlated to soil water content and by soil temperature. After its production, CH<sub>4</sub> migrates to the soil surface and is emitted to the atmosphere through three main processes (Bridgman et al., 2013): (1) diffusion through porous soil media; (2) ebullition, bubbles form in pores filled with water then quickly migrate to the surface; (3) plant-mediated fluxes via some vascular plant adapted to live in flooded environments. These plants developed aerenchyma to channel gas fluxes, oxygen is transported to roots and cells and CH<sub>4</sub> is 95 transported from roots to the atmosphere (Bridgman et al., 2013; Smith et al., 2003).

Since the late 1980's, most of the CH<sub>4</sub> cycling processes has been mathematically described and included in terrestrial ecosystem models (Xu et al., 2016). These terrestrial ecosystems models have been outlined into two broad categories by Xu et al. (2016) review: (1) empirical models employed to evaluate observed processes of the CH<sub>4</sub> cycling and (2) process-based models used for budget quantification and to study sensitivity of CH<sub>4</sub> processes to environmental drivers. 100 However, so far only few global scale models feature peatland ecosystems, permafrost dynamics and CH<sub>4</sub> fluxes which are essential features to evaluate future climate changes and interactions between land surface and the atmospheres (Anav et al., 2013). Recent developments of ORCHIDEE land surface model lead to simulate soil hydrology, permafrost thermodynamic and carbon cycle in the northern latitudes (Guimberteau et al., 2018) and in the northern peatland specifically (Qiu et al.), including peat carbon decomposition controlled by soil water content and temperature as well as CO<sub>2</sub> production and 105 consumption processes (Largergeron et al., 2018; Qiu et al., 2018). In the present study we adapt the Khvorostyanov et al. (2008a, 2008b) methane model to ORCHIDEE-PEAT (section 2.1) and calibrate and evaluate simulated emissions at northern peatland sites. To achieve this revised model calibration, parameters were optimized with a data assimilation approach described in section 2.3. Parameters were optimized against methane fluxes at each site and from multiple sites simultaneously (section 3) in order to highlight parameter uncertainties while scaling up simulations from site to larger scale. 110 The model evaluation is performed by discussing both optimization methods.



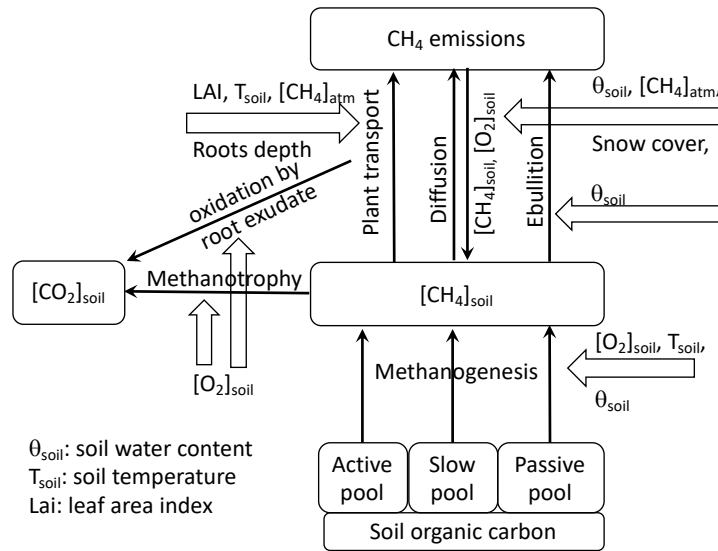
## 2 Model description

### 2.1 ORCHIDEE-PCH4

The ORCHIDEE land surface model is a dynamic global process-oriented model that simulates carbon, water and energy fluxes between the biosphere, the land surface geosphere and the atmosphere. The carbon scheme describes photosynthesis, respiration, soil carbon cycle and CO<sub>2</sub> production and emissions. One of the branches of the ORCHIDEE land model aimed to improve the implementation of high latitude physical, hydrological and biogeochemical processes such as soil thermal processes, hydraulic processes, snowpack properties, and plant and soil carbon fluxes (ORCHIDEE-MICT, Guimberteau et al., 2018).

A northern peatlands scheme has been recently included to the model (ORCHIDEE-PEAT, Llargeron et al., 2018; Qiu et al., 2018) which includes a peatland PFT (plant functional type) with adapted biological parameters was created allowing a separate calculation of the water balance. This PFT is defined as a flood tolerant C<sub>3</sub> grass with reduced productivity due to the lack of nutrients, and with a reduced rooting depth. For the present study, the ORCHIDEE-PEAT v2.0 (Qiu et al., 2019) has been enriched with a module simulating methane production, oxidation and transport in northern peatlands and named ORCHIDEE-PCH4. To achieve this, the methane scheme described by Khvorostyanov et al., (2008a, 2008b) has been revised according to high latitude processes and peatland ecosystem features. This early version was an idealized 1D soil model that accounted for heat and gas transport and soil organic carbon decomposition and production of CO<sub>2</sub> and CH<sub>4</sub> driven by soil water content and temperature in the soil column. In that early version, only a moss layer that serves as a thermal insulator was considered for the vegetation above ground (Khvorostyanov et al., (2008a). Soil humidity and carbon dynamic were treated by a single layer bucket scheme of 1 m depth and containing a fixed amount of soil carbon content. In contrast, the ORCHIDEE-PCH4 is integrated into the peatland soil hydrological diffusion model (Llargeron et al., 2018; Qiu et al., 2018) that incorporates water supply by precipitations and by runoff collected from other soils surrounding the peatland in the same grid-cell. The deep drainage is blocked to maintain soil water content at saturation in the bottom part of the peat soil. At the top of the water column, a dynamic water reservoir was added to represent standing water above the soil surface when water inputs exceed outputs and that soil is fully saturated. ORCHIDEE-PEAT simulates peat accumulation and decomposition to CO<sub>2</sub>, of the three soil carbon pools, active, slow and passive that are vertically discretized in 32 layers accounting for a total maximum depth of 38 m (Qiu et al., 2019).

The methane scheme summarized in Figure 1, delineates (1) methanogenesis of the three carbon pools, (2) methane and oxygen transport in the soil and snow layers, (3) transport of methane to the atmosphere by ebullition, (4) plant mediated transport and (5) methanotrophy by soil oxic conditions and roots exudates. Implementation of methane production and oxidation and transport are specified respectively in sections 2.1.1 and 2.1.2 whereas parameters values established for formatting site simulations conditions before the observation periods are given in section 2.2. Then, section 2.3 describes the parameter optimization approaches.



145 **Figure 1: Model diagram of methane cycling processes in ORCHIDEE-PCH4. Carbon fluxes are indicated by thin black arrows. Other variables that influence each carbon flux are displayed on white arrows.**

Each of these processes are constrained by soil temperature, soil water content ( $\theta_{soil}$ ), soil  $O_2$  concentration, atmospheric  $CH_4$  concentration, leaf area and snow cover. The temporal variation of  $CH_4$  in the soil layer  $z$  is assessed by:

$$\frac{\partial [CH_4](z,t)}{\partial t} = f_{MGa} + f_{MGs} + f_{MGp} - f_{Diff} - f_{Ebu} - f_{PMT} - f_{MT}, \quad (1)$$

150 where each term expresses methane production ( $f_{MG}$ , MG: methanogenesis), transport by diffusion, ebullition, and plants ( $f_{Diff}$ ,  $f_{Ebu}$ ,  $f_{PMT}$ ) and oxidation ( $f_{MT}$ , MT: methanotrophy) processes. Net methane fluxes to the atmosphere is the sum of methane transport processes  $f_{Ebu}$  (Ebu:ebullition) and  $f_{PMT}$  (PMT: plant mediated transport) and the amount of  $CH_4$  that diffuses from the top soil layer at  $z = 0$  to the atmosphere. Prognostic variables are defined per air volume which is the volume of gas in the air-filled pores ( $v$ ) and gas dissolved in the water-filled pores (Khvorostyanov et al., 2008; Tans, 1998; Tang et al., 2013; Tang and Riley, 2014) assuming a constant equilibrium between gas concentrations in the air-filled and the water-filled part of pores. This gas volume is linked to the soil volume by the total  $CH_4$  and  $O_2$  in pores ( $\epsilon_{gas}$ ,  $gas=O_2, CH_4$ ) defined as:

$$\epsilon_{gas} = v + \theta_{soil} \pi_{soil} B_{gas}, \quad (2)$$

160 where  $\theta_{soil}$  is the volumetric water content of the soil,  $\pi_{soil}$  is the soil porosity and  $B_{gas}$  is the Bunsen gas solubility coefficient defined for  $CH_4$  and  $O_2$ , respectively, with  $B_{CH_4}=0.043$  and  $B_{O_2}=0.038$  (Hodgman, 1960; Wiesenburg and Guinasso, 1979).



### 2.1.1 Methane production and oxidation

Methanogenesis in soil occurs when oxygen concentration is limited for microorganisms and is considered for each type of soil carbon pools ( $[C]_i$ ,  $i = a, s, p$ ), active, slow and passive:

$$165 \quad f_{MG_i} = [C]_i \frac{k_i}{q_{MG}} e^{-O_{2,p}/O_2^*} f_{clay}, \quad (3)$$

where the rate of methanogenesis ( $k_i$ ) depends on soil temperature and humidity according to the same function as for heterotrophic respiration (Qiu et al., 2019). This rate has been defined by (Khvorostyanov et al., 2008a) to be 10 times lower than the rate of heterotrophic respiration. Here,  $q_{MG}$  determine the ratio between both rate of soil oxic and anoxic decomposition,  $O_{2,p}$  is the oxygen concentration in the soil per unit porous volume,  $O_2^*$  is the soil oxygen concentration at  
 170 which anoxic conditions are reached and enable methane production. This oxygen concentration threshold is assumed to be 2 g m<sup>-3</sup> (Duval and Goodwin, 2000). Soil clay content affects the decomposition of the active soil carbon pool (Parton et al., 1988):

$$f_{clay} = 1 - (0.75 \text{ clay}), \quad (4)$$

where clay is the clay content, neither the slow nor the passive pools are modified by  $f_{clay}$ . Methane is oxidized to  
 175 CO<sub>2</sub> in aerated soil layers. The amount of methane consumed by methanotrophy is limited by the soil oxygen concentration following a 1:2 CH<sub>4</sub>:O<sub>2</sub> molar ratio:

$$f_{MT} = k_{MT} \frac{1}{2} [O_2]_{soil} \frac{Mw_{CH_4} \epsilon_{O_2}}{Mw_{O_2} \epsilon_{CH_4}}, \quad (5)$$

where  $k_{MT}$  is the rate of methanotrophy which value range from 1.4 hours to 5days (Morel et al., 2019), the conversion of oxygen to methane content is provided by methane and oxygen molecular weight  $Mw_{CH_4}$  and  $Mw_{O_2}$  and their  
 180 respective total gas porosities  $\epsilon_{CH_4}$  and  $\epsilon_{O_2}$ .

### 2.1.2 Methane transport

The formation of methane bubbles in water-filled pores is determined by:

$$f_{Ebu} = k_{Ebu} ([CH_4]_{soil} - [CH_4]_{ET}) p_{Ebu}, \quad (6)$$

where  $k_{Ebu}$  is a rate constant of 1h<sup>-1</sup>, methane ebullition occurs when methane concentration exceeds a concentration  
 185 threshold that depend on soil temperature ( $T_{soil}$ ) and pressure ( $P_{soil}$ ) above 0.75m depth as follow:

$$[CH_4]_{ET} = \frac{m_{wCH_4} P_{soil} Mw_{CH_4}}{RR T_{soil} B_{CH_4}}, \quad (7)$$

where  $m_{wCH_4}$  is the methane mixing ratio in the bubbles. Walter and Heimann, (2000) determined this mixing ratio to range between 27 and 53% for totally vegetated and unvegetated soil and Riley et al. (2011) at 15%. It is converted to



190 gCH<sub>4</sub> per unit porous volume by RR the ideal gas constant, M<sub>wCH<sub>4</sub></sub> and B<sub>CH<sub>4</sub></sub> the Bunsen methane solubility coefficients. It has been suggested that ebullition in soil occurs when the partial pressure of dissolved gases exceeds the hydrostatic pressure (Chanton and Whiting, 1995). We estimated that in our model below the layer corresponding to 0.75 m the hydrostatic pressure is always higher than the partial pressure of dissolved gases. Therefore, we considered below 0.75 m that methane ebullition threshold is constant and equal to the value defined at 0.75 m in order to avoid methane accumulation in the deeper layers. The methane flux provided by ebullition (f<sub>Ebu</sub>) is modulated by the probability of methane bubbles to reach the soil surface. Indeed, in the soil column the water table level fluctuates modifying the connectivity between water-filled pores involving variation of the surface methane flux. Therefore, the probability that methane bubbles escape to the atmosphere is expressed as:

$$p_{Ebu} = \theta_{soil}(z)^{\frac{\Delta z}{wsize \times \eta}}, \quad (8)$$

200 where  $\theta_{soil}(z)$  is the soil water content,  $\Delta z$  is the soil layer thickness and the tortuosity  $\eta$  that depicts the sinuous path of bubbles. The term  $wsize$  sizes the extent of the connected network of water-filled pores envisioned that can be depicted as of droplets dispersed in the pores. Khvorostyanov et al., (2008a, 2008b) defined it for a carbon rich loess deposit of the Yedoma to 1 cm.

In wetlands, some vascular plants developed a strategy to carry oxygen down to their root tips employing aerenchyma tissue. These tissues are air-channels in which gas exchange depending on gas concentrations gradient between the soil and the atmosphere. Oxygen is transferred from the atmosphere to the roots and creates an aerobic zone around them in which methane will be oxidized. The proportion of methane oxidized in the root oxygenated zone (M<sub>rox</sub>) ranging of 39 and 98% Walter and Heimann, (2000) is emitted as CO<sub>2</sub> to the atmosphere. Conversely, the methane concentration gradient results in a flux to the atmosphere through plants that is expressed by:

$$f_{PMT} = k_{PMT} \times T_{veg} \times f_{root} \times LAI \times ([CH_4]_{soil} - [CH_4]_{atm}) \times (1 - M_{rox}), \quad (9)$$

210 where  $k_{PMT}$  is a rate constant of the unit 0.01 h<sup>-1</sup> and  $T_{veg}$  has been defined by Walter and Heimann, (2000) as a factor that describes the efficiency of plants in methane transport depending on the type and the density of these plants. Its value ranges between 0-15 with shrubs and trees being poorly efficient and grasses and sedges being very efficient in gas transport. Methane concentration gradient is also modified by the vertical distribution of roots in the soil as:

$$f_{root} = 2 \times \left( \frac{z_{root} - z_{soil}}{z_{root}} \right), \quad (10)$$

215 This function describes a linear relationship between root biomass and soil depth in which  $z_{root}$  is the rooting depth and  $z_{soil}$  the soil depth. The leaf area index (LAI) influences the methane flux depending on the growing stage of the plants.

The gas diffusion scheme considered (1) the diffusion of oxygen from the top soil to the soil layer, (2) the diffusion of methane produced and remaining in the soil and (3) methane exchange between the soil and the atmosphere at  $z=0$ :





$$f_{Diff} = D_{gas}(z) \frac{\partial [gas]_{soil}(t,z)}{\partial z}, \quad (11)$$

220 Diffusion coefficients,  $D_{gas}$ , are based on the diffusivity of each gas in air ( $D_{gas, air}$ ) and in water ( $D_{gas, water}$ ):

$$D_{gas} = (D_{gas,air} v + D_{gas,water} \theta_{soil} \pi_{soil} B_{gas}) \eta, \quad (12)$$

where  $v$  is the volume of gas in the air-filled pores,  $\theta_{soil}$  is the volumetric water content of soil,  $\pi_{soil}$  is the soil porosity and  $B_{gas}$  is the Bunsen coefficient of the gas, the tortuosity  $\eta$  is defined to be  $2/3$  (Hillel, 1982). Diffusivity of  $O_2$  in air and in water are defined respectively to  $1.6 \times 10^{-5}$  and  $1.6 \times 10^{-9}$   $m^2/s$  and for methane  $1.7 \times 10^{-5}$  and  $2.0 \times 10^{-9}$   $m^2/s$ . The  
225 diffusion is discretized using a forward time centered space method (Press et al., 1997) and converted in a tridiagonal system of equations before being solved using forward then backward substitution method. A time-splitting option is also implemented for the diffusion of large concentrations of gas per time step.

The only source of oxygen considered is from the atmosphere and is determined using atmospheric surface pressure, temperature and an atmospheric  $O_2$  mixing ratio of 20.9%. Atmospheric methane content is also defined in the  
230 same way employing a methane mixing ratio of 1.7 ppm and is used as a boundary condition when the topsoil layer is in contact with the atmosphere. In winter, when snow accumulates above the topsoil, these atmospheric boundary conditions are applied to the top snow layer then gases diffuse from and to the atmosphere through the snow layers then soil layers. Methane and oxygen diffusivity in the snow are defined by:

$$D_{gas} = D_{gas,air} \left( 1 - \frac{\rho_{snow}}{\rho_{ice}} \right) \eta_{snow}, \quad (13)$$

235 where  $D_{gas,air}$  the diffusion coefficient of each gas in free air, the snow porosity that is defined by the ratio of density of snow  $\rho_{snow}$  and ice  $\rho_{ice}$  and the tortuosity ( $\eta_{snow}$ ) is equal to  $\sqrt[3]{\left( 1 - \frac{\rho_{snow}}{\rho_{ice}} \right)}$ . Snow density is determined by the snowpack scheme (Wang et al., 2013) and the density of the ice is  $920.0 \text{ kg/m}^3$ .

## 2.2 Sites description and simulation setup

240 The model was evaluated on 14 peatland sites distributed on the Eurasian and American continents in boreal and temperate northern regions (from  $41^\circ N$  to  $69^\circ N$ ). These sites are a subset of the 30 peatlands sites collected for the calibration of ORCHIDEE-PEAT (Qiu et al., 2018) for which, in addition of eddy-covariance data and physical variables (water table, snow depth, soil temperature), methane emissions were measured by eddy-covariance or chamber measurements (for FR-Lag and RU-Che). A description of each of these sites is available in Qiu et al., (2018). In Table 1,  
245 sites are assembled by increasing extreme values of mean monthly measurements of methane emission then by locations and ecological characteristics. The extreme values of mean monthly measurements are the most reliable quantity of methane fluxes since periods of observation and monitoring frequency differ. Among the 14 peatlands, 9 sites are located in temperate regions, 3 in boreal regions and 2 in arctic permafrost regions. The majority of the sites are fen (9 sites) and the others are 3 bogs (DE-Sfn, US-Bog, DE-Hmm), a marsh (US-Wpt) and a tundra (RU-Che). It is worth noticing that there is no obvious



250 correlation between the magnitude of the monthly mean fluxes and types of ecosystem. Indeed, US-Los and DE-Spw are  
 temperate fens and release less than  $10 \text{ mg CH}_4 \text{ m}^{-2} \text{ d}^{-1}$ . Sites emitting between 10 and  $150 \text{ mg m}^{-2} \text{ d}^{-1}$  are located in  
 Germany, Northwestern America and France among which half are fens and the other half are bogs. Half of them, DE-Sfn,  
 US-Bog and CA-Wp1 are forested peatlands and release less than  $55 \text{ mg CH}_4 \text{ m}^{-2} \text{ d}^{-1}$ . While the others, DE-Zrk, DE-Hmm  
 and FR-Lag experienced a temporary drainage event because of anthropogenic activities during years earlier than the  
 255 observed period. Sites located in Finland, Denmark and Poland are fens emitting between 150 and  $400 \text{ mg m}^{-2} \text{ d}^{-1}$ . The  
 largest methane emitters are the arctic tundra RU-Che and the marsh US-Wpt which released more than  $500 \text{ mg m}^{-2} \text{ d}^{-1}$ . All  
 sites are covered with some snow during winter and US-Bog and RU-Che are overlaid with permafrost located below 0.5  
 meter.

260 **Table 1. Sites ecological characteristics summary. Sites identification includes the country initials and the short three letters name  
 of each site, locations of the sites are provided by the country, latitude (Lat) and longitude (Lon) values. Hydrological  
 characteristics are distinguished by the type of ecosystem, fen, bog, tundra and marsh. Y and N indicate presence and absence of  
 snow cover in winter, permafrost soil, forest above the peat. Temporary drawdown of the water table level is specified by presence  
 and absence indicators Y or N. Grey color highlight groups of peatlands organized by amount of methane emissions in ranges 0-  
 10, 10-150, 150-400, 400-600  $\text{mg m}^{-2} \text{ d}^{-1}$ .**

Sites	Site name	Country	Lat	Lon	Climatic zone	Types	Observed period (year range)	Monthly mean methane emissions ( $\text{mg m}^{-2} \text{ d}^{-1}$ , min, max)	Forest (Y/N)	Drained (Y/N)	Snow (Y/N)	Permafrost (active layer depth in m, Y/N)
US-Los	Lost Creek	United States	46.08	-89.98	temperate	fen	2006	-1.1, 3.6	N	Y	Y	N
DE-Spw	Spreewald	Germany	51.89	14.03	temperate	fen	2011	-1.4, 6.5	Y	N	Y	N
DE-Sfn	Schechenfilz Nord	Germany	47.81	11.33	temperate	bog	2012-2014	4.7, 38.0	Y	N	Y	N
DE-Zrk	Zarnekow	Germany	53.88	12.89	temperate	fen	2013	0, 37.9	N	Y	Y	N
CA-Wp1	AB-Western Peatland	Canada	54.95	-112.47	boreal	fen	2007	0, 49.3	Y	N	Y	N
US-Bog	Bog at Bonanza Creek	United States	64.7	-148.32	boreal	bog	2013	0, 54.4	Y	N	Y	Y (0.5-0.9)
FR-Lag	LaGuette	France	47.3	2.3	temperate	fen	2014-2016	0, 99.2	N	Y	Y	N
DE-Hmm	Himmelmoor	Germany	53.74	9.85	temperate	bog	2012-2014	0, 151.0	N	Y	Y	N
FI-Lom	Lompolojänkka	Finland	68	24.21	boreal	fen	2012-2014	0, 187.8	N	N	Y	N
DK-NuF	Nuuk Fen	Denmark	64.13	-51.39	arctic	fen	2006-2009	6.1, 232.2	N	N	Y	N
PL-Kpt	Kopytkowo	Poland	53.59	22.89	temperate	fen	2013-2015	2.2, 294.7	N	N	Y	N
PL-Wet	Polwet	Poland	52.76	16.31	temperate	fen	2013	0, 361.6	N	N	Y	N
US-Wpt	Winous Point North Marsh	United States	41.46	-83	temperate	marsh	2011-2013	6.1, 502.9	N	N	Y	N
RU-Che	Cherski	Russia	68.61	161.34	arctic	tundra	2002-2005	0, 565.3	N	N	Y	Y (0.5)



265

270

275

280

Each peatland site is simulated in a 0.5° grid cell considering a peatland fraction defined in Table 2. The proportion of peatlands per grid cell was defined by modifying prescribed values employed by Qiu et al., (2018) in order to collect enough water to fill the peatland by runoff from the other soil fractions and adjust the water table level to match the observed level. We employed vegetation phenotype properties and peatland fractions described in (Qiu et al., 2019) and peatlands hydrology and carbon model as described in (Qiu et al., 2019). Site simulations were then constrained with a half hourly time series of meteorological conditions e.g. air temperature, wind speed, wind direction, longwave incoming radiation, shortwave incoming radiation, specific humidity, atmospheric pressure, and precipitation. These time series are flux tower measurements that were gap filled by 6-hourly CRU-NCEP 0.5° global climate forcing dataset (Qiu et al., 2018). Other variables measured on a half-hourly time step at sites e.g. CO<sub>2</sub> and energy (latent heat: LE; sensible heat: H) fluxes, water table position, soil temperature, and snow depth served for the calibration of peatland soil and vegetation phenotype characteristics such as the maximum rate of carboxylation (V<sub>cmax</sub>). Optimized V<sub>cmax</sub> values (Qiu et al., 2018) are utilized to capture spatial carbon fluxes gradients (gross primary production, ecosystem respiration and net ecosystem exchange) at each peatland site. Simulations with ORCHIDEE-PCH<sub>4</sub> driven by repeated site-specific meteorological conditions were performed for various periods of time to reach the observed soil carbon content and maximum peat depth (Table 2).

**Table 2. Simulations conditions and framework to constrain peatlands soil carbon stock. Grey color reports the groups of sites with equivalent levels of methane emissions (Table 1).**

Sites identification	Peat fraction	V <sub>cmax</sub>	Carbon accumulation period	Maximum peat depth		Soil carbon stock	
				Observed	Simulated	Observed	Simulated
	fraction	μmol m <sup>-2</sup> s <sup>-1</sup>	numbers of years	m	m	kg/m <sup>2</sup>	kg/m <sup>2</sup>
US-Los	0.16	65	214	0.5	0.75	27.5	28.0
DE-Spw	0.14	89	272	1.2	1.5	84.0	84.2
DE-Sfn	0.18	45	4 544	5	5	372.8	372.5
DE-Zrk	0.9	33	10 060	10	7	696.7	696.6
CA-Wp1	0.16	38	620	2	2	51.0	51.0
US-Bog	0.27	42	4 305	2	3	207.4	207.7
FR-Lag	0.22	42	937	1.6	2	121.0	121.4
DE-Hmm	0.9	35	8 963	3	3	265.0	266.4
FI-Lom	0.27	28	6 396	3	3	200.3	200.5
DK-NuF	0.5	31	8 959	0.75	1.5	54.6	54.6
PL-Kpt	0.14	52	3 819	2.5	3	250.0	250.3
PL-Wet	0.11	52	261	0.5	0.75	37.6	37.8



US-Wpt	0.27	80	32	0.3	0.75	5.3	5.4
RU-Che	0.05	35	2 968	0.56	0.75	45.8	45.8

285 During the first part of those simulations, atmospheric CO<sub>2</sub> concentration was set to preindustrial value at 285 ppm then between 1860 until the beginning of the respective observation period of methane emissions listed in Table 1, CO<sub>2</sub> concentration had risen. During soil carbon accumulation simulations, methane model parameters were defined to the default values defined in Table 3. Then during the site-specific measurement periods (Table 1), methane variables are calibrated against observed monthly average methane fluxes times series and driven.

**Table 3. List of parameters driving the methane production, oxidation and transport scheme in ORCHIDEE-PCH4.**

Parameters	Description	Unit	default values	ranges	References
q <sub>MG</sub>	Ratio of soil oxic and anoxic decomposition	proportion	10.0	9.0, 11.0	Khvorostyanov et al., 2008a, Wania et al. 2010
k <sub>MT</sub>	Methanotrophy rate	1/d	5.0	1.0, 5.0	Khvorostyanov et al., 2008a ; Morel et al., 2018
M <sub>rox</sub>	Root methane oxidation	fraction	0.5	0.0, 1.0	Walter and Heimann, 2000
Z <sub>root</sub>	Root depth	m	0.3	0.01, 0.5	Walter and Heimann, 2000
T <sub>veg</sub>	The efficiency of methane plant mediated transport	proportion	7.0	0.0, 15.0	Walter and Heimann, 2000
wsize	Connectivity of soil humidity	m	0.01	0.001, 0.1	Khvorostyanov et al., 2008a
m <sub>XTCH4</sub>	Methane mixing ratio in bubbles	fraction	0.27	0.05, 0.53	Morel et al., 2018

290

### 2.3 Optimization of methane parameters

295 The methane scheme revisited in ORCHIDEE-PCH4 (described in section 2.1) is driven by 7 parameters (Table 3) that constrain methane production (q<sub>MG</sub>), oxidation (k<sub>MT</sub>, M<sub>rox</sub>) and transport (m<sub>wTCH4</sub>, wsize, T<sub>veg</sub>, Z<sub>root</sub>). In order to optimize these parameters, we employed the ORCHIDEE data assimilation system (Bastrikov et al., 2018) that relies on the minimization of a cost function employing a Bayesian statistical formalism that expresses the discrepancy between observations and simulated methane emissions and the difference between the optimized parameter values and the prior information on them, weighted by the uncertainties assigned to both observations and parameters. A random search algorithm based on the genetic algorithm (GA) serves to randomly iterate the set of seven parameters following the principles of genetics and natural selection similar to chromosome genetic sequencing (Goldberg, 1989; Haupt and Haupt,



300 2004). At each iteration, 8 sets of parameters are defined from the previous iteration following crossover and mutation rules (Bastrikov et al., 2018). The frequency at which these rules are used, is governed by the crossover/mutation ratio fixed to 4 : 1, the number of parameter blocks exchanged during crossover that is 2 and the number of parameters perturbed during mutation that is equal to 1. In addition, a ranking in ascending order of the corresponding cost function values of all sets of parameters serves to selectively preserve the set of parameters that reduce the gap between observation and simulation data.

305 Two types of simulations are performed: single site experiment for which parameters are optimized for each site and a multi-site experiment that aims at refining one set of parameters considering all sites together. The single site experiments are performed for 100 iterations and aim at finding the lowest cost function employing the model–data root mean square difference (RMSD). Prior conditions for the single site experiment are described and listed in Table 3. Initial parameters values and range were derived from literature and of expert knowledge and parameter uncertainties are defined as 40% of the prescribed ranges. Across sites, mean values of each parameter serve as prior conditions for the multi-site experiment. This later was performed for 50 iterations and aims to evaluate methane emissions uncertainties at hemispheric-scale when only one set of parameters is employed.

310

### 3 Results

#### 3.1 Single site optimization

315 For each site, to minimize the discrepancy between observed and simulated methane emissions, iterative single site simulations were performed. Successive runs serve to ensure that the minimum reach is not a local minimum. Results from the last minimization experience are reported in Table 4. As expected, most optimized parameters fit within the initial range defined in Table 3 except for four of the sites. One of these four sites, DE-Spw, is among the sites that emitting the fewest amount of methane (up to  $7 \text{ mg m}^{-2} \text{ d}^{-1}$ ) and features a larger stock of carbon of  $84 \text{ kg C / m}^2$  than at US-Los that features  $27 \text{ kgC / m}^2$  and emits up to  $4 \text{ mg m}^{-2} \text{ d}^{-1}$ . This explains, at the DE-Spw site, that the optimized value of  $w_{\text{size}}$  was reduced to  $0.5 \text{ mm}$  to maintain low methane emissions. The other three sites for which some of the optimized parameters are out of the initial range, DK-Nuf, PL-Wet and US-Wpt, are among the sites that emit more than  $150 \text{ mg CH}_4 \text{ m}^{-2} \text{ d}^{-1}$ . The carbon stock at DK-Nuf and PL-Wet are respectively  $55$  and  $38 \text{ kg C / m}^2$  which is lower than at FI-Lom and PL-Kpt that accumulated more than  $200 \text{ kg C / m}^2$ . Three parameter ranges were modified for DK-Nuf, the minimum value of  $q_{\text{MG}}$  was lowered to  $7.0$ ,  $z_{\text{root}}$  maximum is increased to the maximum peat depth at  $0.75\text{m}$ , the maximum value of  $T_{\text{veg}}$  was increased to  $40.0$  and the maximum rate of methanotrophy  $k_{\text{MT}}$  was enlarged up to  $8 \text{ d}^{-1}$  in order to obtain in the simulation methane emissions higher than  $150 \text{ mg CH}_4 \text{ m}^{-2} \text{ d}^{-1}$ . PL-Wet required also to modify range values of  $q_{\text{MG}}$  to  $1.0\text{-}11.0$  leading to the lowest optimized  $q_{\text{MG}}$  value of  $4.0$  which significantly reduced the RMSD from  $227.4$  to  $80.5$  (Fig. S1 and Table S1). For the US-Wpt site,  $q_{\text{MG}}$ ,  $k_{\text{MT}}$  and  $T_{\text{veg}}$  were adjusted to increase methane production and fluxes in order to balance the carbon stock of  $5 \text{ kg C / m}^2$  that is lower than the one at RU-Che.

320

325

330



**Table 4. Single site optimized values of methane scheme parameters for each peatland site. In parenthesis are indicated prior parameter ranges which differ from the values in Table 3. Uncertainties for these ranges are specified in parentheses.**

Sites	q <sub>MG</sub>	k <sub>MT</sub>	M <sub>rox</sub>	Z <sub>root</sub>	T <sub>veg</sub>	wsize	m <sub>xCH<sub>4</sub></sub>
	proportion	1/d	fraction	m	proportion	m	fraction
US-Los	9.9	1.92	0.994	0.057	3.8	0.0319	0.306
DE-spw	9.9	1.00	0.595	0.188	0.003	0.0005	0.530
DE-Sfn	10.5	1.98	0.493	0.399	0.01	0.0010	0.377
DE-Zrk	10.0	1.98	0.756	0.418	9.8	0.0015	0.259
CA-Wp1	10.2	2.99	0.471	0.122	0.45	0.0059	0.193
US-Bog	9.2	2.45	0.500	0.173	4.4	0.0098	0.117
FR-Lag	10.7	1.74	0.857	0.291	0.5	0.0085	0.463
DE-Hmm	9.4	3.94	0.147	0.118	3.7	0.0011	0.164
FI-Lom	9.5	3.97	0.491	0.174	5.7	0.0040	0.140
DK-NuF	8.5 (7.0, 11.0)	4.38	0.068	0.677 (0.01,0.75)	23.6 (0.0, 40.0)	0.0255	0.203
PL-Kpt	10.3	1.32	0.541	0.071	9.1	0.0030	0.061
PL-Wet	4.0	1.95	0.165	0.328	6.0	0.0110	0.136
US-Wpt	7.9 (7.0, 11.0)	5.25 (1.0, 8.1)	0.035	0.304	22.3 (0.0, 40.0)	0.0023	0.120
RU-Che	9.8	1.36	0.004	0.404	8.4	0.0171	0.294
Uncertainty	0.8 (1.6)	1.6 (2.8)	0.4	0.196 (0.296)	6.0 (16.0)	0.0398	0.192

335

Across sites, q<sub>MG</sub> values extend between 7.9 and 10.7, optimized k<sub>MT</sub> values vary between 1 and 5.25 d<sup>-1</sup>. The fraction of methane that is oxidized at the root (M<sub>rox</sub>) level fluctuate between 0.004 and 0.99 with the lowest values obtained at US-Wpt and RU-Che sites that emitted up to 500 mg CH<sub>4</sub> m<sup>-2</sup> d<sup>-1</sup> and the largest values at US-Los that released the fewest amount of methane. The optimization of the maximum root depth (Z<sub>root</sub>) results in values ranging between 0.057 and 0.68 with a maximum value at the DK-Nuf site which is an arctic fen in Greenland. Optimized values for plant mediated transport efficiency (T<sub>veg</sub>) fell between 0.003 and 23.6. The largest T<sub>veg</sub> values of 23.6 and 22.3, were obtained for DK-Nuf and US-Wpt, respectively and the lowest value of 0.003 at DE-Spw. The dimension of water droplets dispersed in the soil depict the probability of methane rich bubbles to be released to the atmosphere (wsize). The optimized wsize values vary within the range 0.005 and 0.032. And the optimized mixed ratios of methane involved in the ebullition process (m<sub>xCH<sub>4</sub></sub>) are ranging between 0.06 and 0.53.

340

345



350

**Table 5. Discrepancies between observed and simulated methane emissions are quantified by the root mean square difference (RMSD) approach. Minimization efficiency of each test is indicated by the relationship between the prior using default values and posterior RMSD as  $(1 - \text{RMSD}_{\text{post}} / \text{RMSD}_{\text{prior}}) \times 100$ . Normalized root mean square difference (NRMSD) is defined by the RMSD posterior normalized by the annual mean of observed methane emissions.**

Sites	RMSD prior	RMSD posterior	$1 - (\text{RMSD}_{\text{post}} / \text{RMSD}_{\text{prior}})$	Observed emissions annual mean ( $\text{mgCH}_4 \text{ m}^{-2} \text{ d}^{-1}$ )	NRMSD
US-Los	69.6	1.1	0.98	0.1	9.85
DE-spw	687.9	9.5	0.99	0.5	19.00
DE-Sfn	263.3	9.2	0.97	3.9	2.36
DE-Zrk	16.2	4.6	0.71	6.2	0.74
CA-Wp1	73.6	11.8	0.84	8.9	1.32
US-Bog	33.0	6.7	0.80	28.6	0.23
FR-Lag	91.4	23.0	0.75	26.9	0.85
DE-Hmm	34.4	25.3	0.26	21.2	1.19
FI-Lom	44.0	38.3	0.12	25.2	1.52
DK-NuF	44.6	40.1	0.10	52.7	0.76
PL-Kpt	146.5	54.6	0.63	56.1	0.97
PL-Wet	181.3	80.5	0.56	93.2	0.86
US-Wpt	265.5	249.0	0.06	196.0	1.27
RU-che	157.4	139.7	0.11	80.4	1.74

355

360

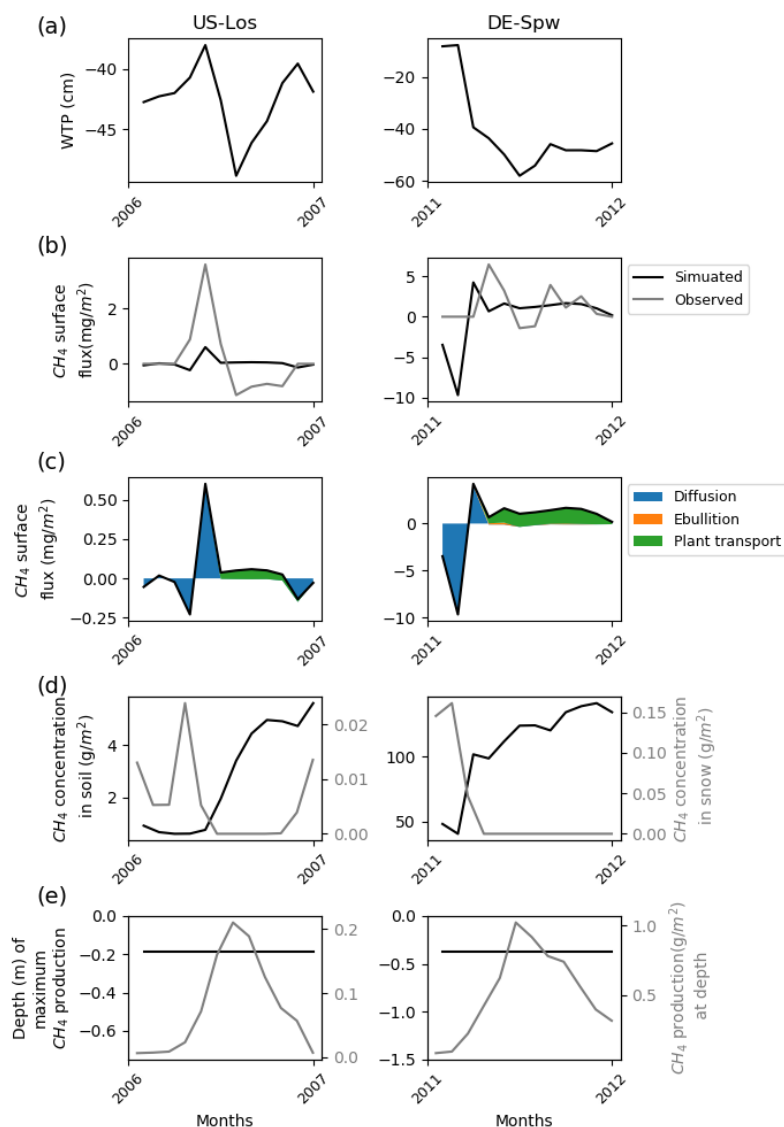
Differences between observed and simulated methane fluxes employing initial and optimized parameters are quantified by the RMSD prior and posterior respectively. At sites where methane fluxes were small such as US-Los and DE-Spw, RMSD posterior values are respectively of 1.1 and 9.5 whereas at US-Wpt and RU-Che where monthly mean methane emissions had reached up to  $550 \text{ mgCH}_4 \text{ m}^{-2} \text{ d}^{-1}$  RMSD posterior are larger i.e. respectively 249 and 140. At sites that emitted between 10 and  $150 \text{ mgCH}_4 \text{ m}^{-2} \text{ d}^{-1}$ , RMSD values fluctuate between 4 and 26 and when methane fluxes were discharged between 150 and  $400 \text{ mgCH}_4 \text{ m}^{-2} \text{ d}^{-1}$ , RMSD is 38 - 80. Performances of the optimization at each site are also evaluated utilizing the relationship  $(1 - \text{RMSD}_{\text{post}} / \text{RMSD}_{\text{prior}}) \times 100$  which compares the RMSD prior defined by using the prior values and ranges and the RMSD posterior obtained after parameters optimization. It might seem that optimizations are more efficient at sites with low methane emissions than at sites that emitted the most whereas NRMSD values which are the RMSD posterior normalized by the annual mean of the observed emissions are close to 1 at each site except for US-Los and DE-Spw for which NRMSD are 10 and 19 respectively. This suggests that the optimizations are less efficient for sites that emitted the least amount of methane. Direct comparison during the period of observation between observed and simulated methane emissions are displayed for each site in Figure 2b, 3b, 4b and 5b. The temporal and the average magnitude are



365 equivalent than in measurements except for the US-Wpt and RU-Che for which simulated emissions are significantly lower than observed emissions.

In addition of the mismatch between observed and simulated methane emissions during the observed period, figures 2, 3, 4 and 5 show the simulated water table position, the amount of methane that is emitted by diffusion, plant transport and ebullition, temporal methane concentration in the soil and in the snow and the depth at which the largest amount of methane is produced together with the rate of production at that depth. These variables show the consistency of the model regarding peatlands functioning. US-Los and DE-Spw were emitting less than  $10 \text{ mg CH}_4 \text{ m}^{-2} \text{ d}^{-1}$  and their simulated water table positions fluctuate below the surface between 10 and 60 cm while showing a clear seasonal pattern and are lower in summer than in winter. In winter, simulated emissions are the result of methane diffusion between the soil and the atmosphere while in spring and summer methane mainly diffuses through aerenchyma of vascular plants. At DE-Spw, simulated methane concentration in the soil that ranges between 40 and  $140 \text{ g/m}^2$ , is more than 10 times higher than at US-Los for which observed concentration barely reaching  $5 \text{ gCH}_4 / \text{m}^2$  in the fall. Model simulates a methane accumulation in the soil at DE-Spw that stimulates a small release of methane to the atmosphere by ebullition. In the model, the largest production of methane occurs consistently around 20 cm for US-Los and 40 cm for DE-Spw which is above the simulated water table position. It is commonly expected for methanogenesis to take place below the observed water table position. However, here the simulated water table position is a prognostic variable defined by the cumulative amount of soil water content over the soil column (Fig. S2 and Fig. S3). Indeed, in these simulations above the water table position soil humidity is still higher than 80% (Fig. S4 and Fig. S5). At those depths the simulated methane productions reach up to respectively 0.2 and  $1.0 \text{ g CH}_4/\text{m}^2$  in the summer. In the winter, simulated methane productions are nearly very small and some methane is diffused in the simulated snow pack covering the peatlands, up to  $0.025 \text{ g CH}_4/\text{m}^2$  at US-Los and  $0.17 \text{ g CH}_4/\text{m}^2$  at DE-Spw. This explains the negative methane flux produced in winter by the model via diffusion of simulated atmospheric methane in the snow cover. Then the positive flux that appears in the spring that occurs simultaneously to snow melting.





390 **Figure 2: Temporal distribution of methane at sites emitting less than  $10\text{mg CH}_4 \text{ m}^{-2} \text{ d}^{-1}$ . (a) Simulated water table position**  
**estimated from the soil water content; (b) Simulated (dark line) and observed (gray line) methane emissions released to the**  
**atmosphere; (c) Cumulative amount of simulated methane emitted by diffusion, plant mediated transport and ebullition; (d)**  
**Methane concentration in the soil layers (dark line) and in the snow layers of the model (gray line); (e) On the left, depth at which**  
 395 **simulated methane production is the highest in the soil, scaled to the maximum peat depth. On the right, the amount of simulated**  
**methane produced at these depths.**

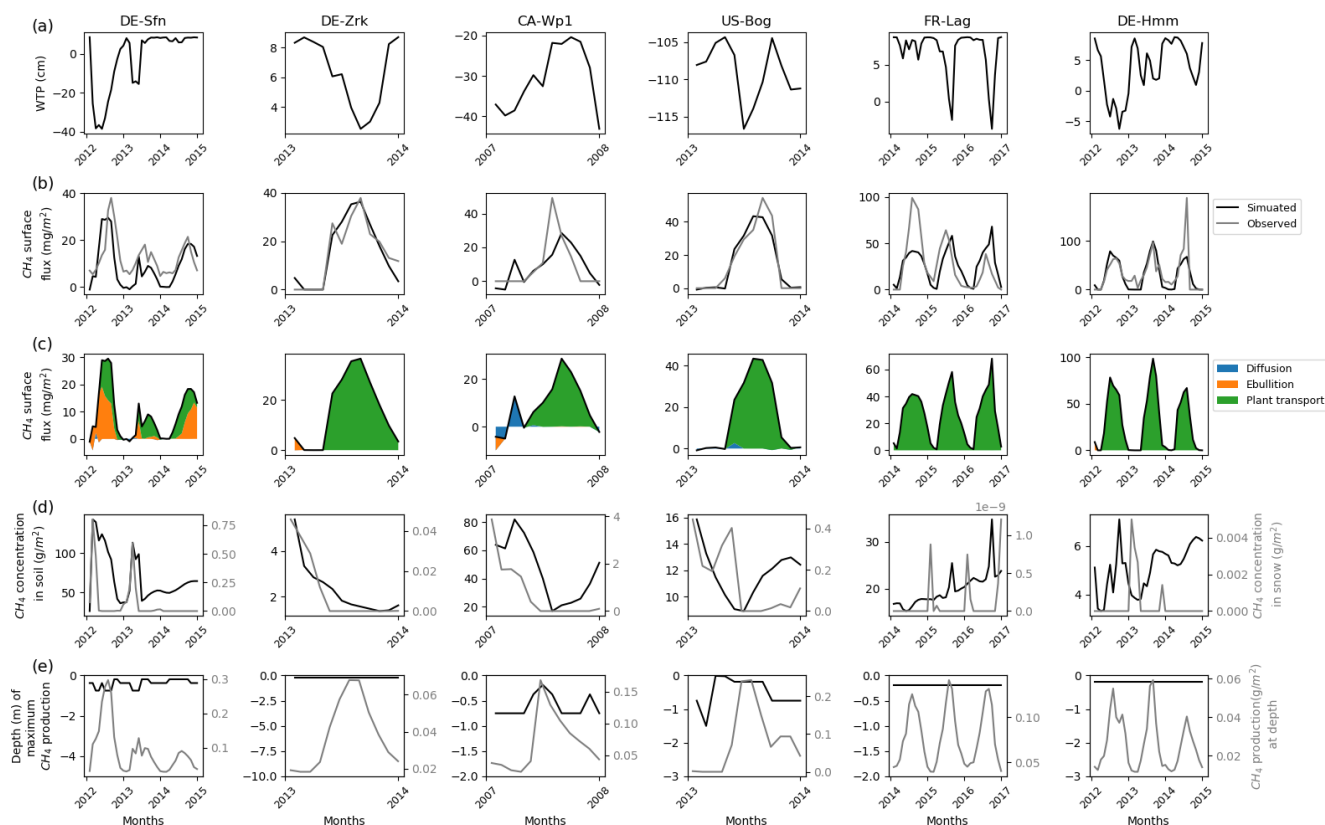
Other sites that emitted less than  $150 \text{ mg CH}_4 \text{ m}^{-2} \text{ d}^{-1}$  are shown in Figure 3. Except for CA-Wp1 and US-Bog, during winter these peatlands are nearly inundated in the simulations with a simulated water table position near 10 cm above ground level. CA-Wp1 and US-Bog are respectively fen and bog boreal peatlands and their simulated water table position is lower than at the other sites. US-Bog is affected by permafrost which might explain the unexpectedly low position of the

400



simulated water table. At DE-Sfn, methane is mainly transported in the model via vascular plants and by ebullition whereas at the other sites, simulated methane is predominantly carried via vascular plants only. As for US-Los and DE-Spw, during the winter simulations show that in the top soil layers some methane is transferred by diffusion to the snow cover. Then a small part of the simulated methane is temporarily stored in the snow and the other part is released to the atmosphere via diffusion. More simulated snow accumulated at DE-Sfn, DE-Zrk, CA-Wp1 and US-Bog where up to 0.8 - 0.04 gCH<sub>4</sub> / m<sup>2</sup> are temporarily stored in the snow. At FR-Lag and DE-Hmm, fewer methane, less than 0.005 gCH<sub>4</sub> / m<sup>2</sup>, are contained in the simulated snow cover that is also scarcer. As for DE-Spw, at DE-Sfn, simulation results show that up to 140 gCH<sub>4</sub> / m<sup>2</sup> accumulate in the soil layers of the model during winter and provide sufficient methane to be expelled to the surface by ebullition. In contrast, methane accumulated up to 80 gCH<sub>4</sub> / m<sup>2</sup> in the soil layers of the model at CA-Wp1 is not sufficient to trigger the methane ebullition process. In all the other sites, methane concentrations in the soil layers of the model are smaller between 5 and 35 gCH<sub>4</sub> / m<sup>2</sup>. The maximum of simulated methanogenesis takes place steadily at around 20 cm depth at DE-Sfn, FR-Lag and DE-Hmm which is in winter about 30cm under the simulated water table position. At this depth simulated methane production fluctuated at 0.01-0.12 gCH<sub>4</sub> / m<sup>2</sup>. At DE-Sfn, CA-Wp1 and US-Bog, simulations show that in the winter most of the methane is produced at around 75 cm depth then in spring and summer the depth of maximum simulated production becomes shallower to reach 20 cm. Early spring at US-Bog, temporarily the maximum simulated production is near the surface at 1cm depth which correlates with an increase of methane that accumulates in the simulated snow. At DE-Sfn, the depth at which the maximum simulated production occurred fluctuates more than at both other sites, CA-Wp1 and US-Bog. Unlike CA-Wp1 and US-Bog, during the first two years the maximum simulated production deepens at 75 cm when the maximum value of simulated production is reached.

420

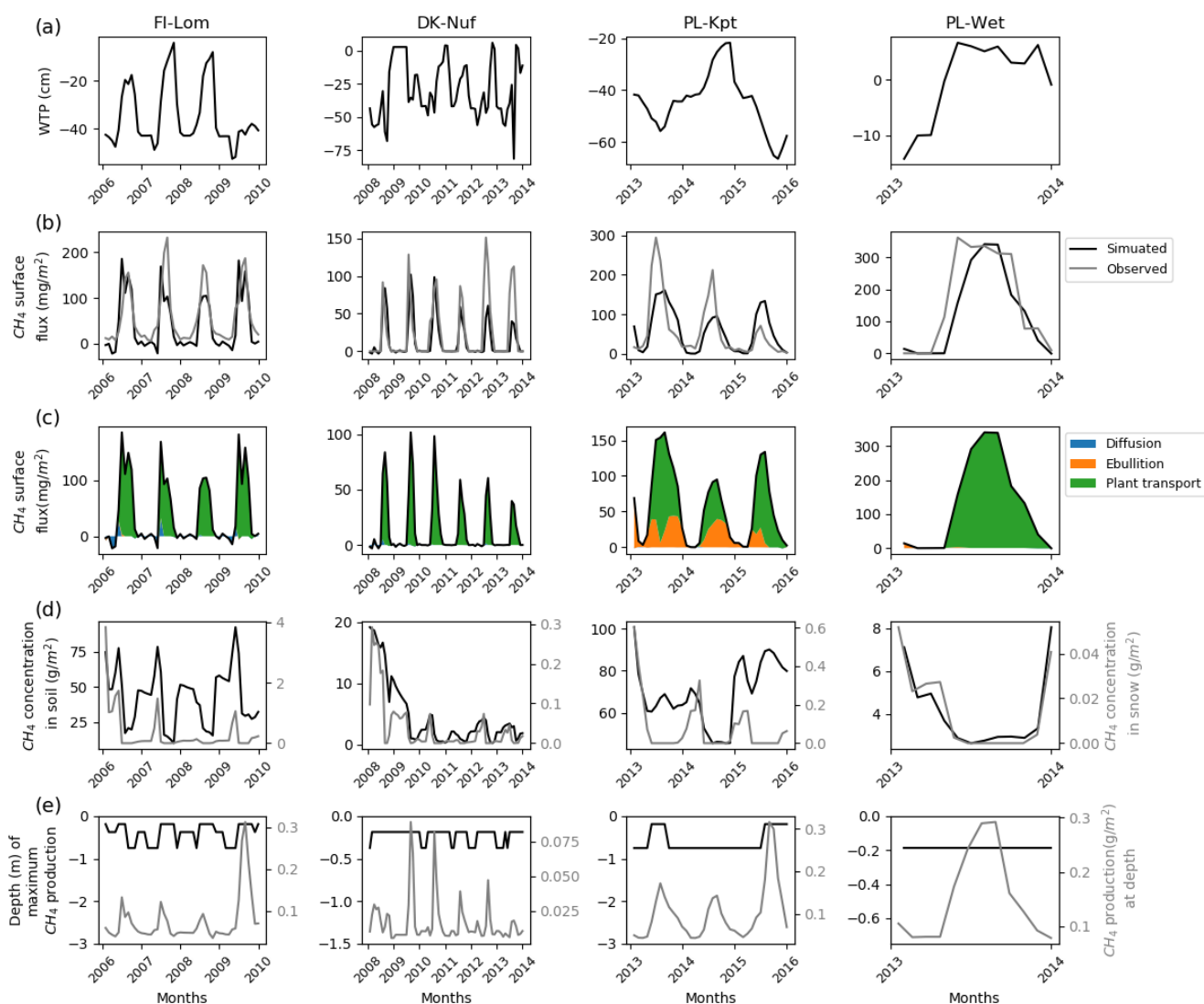


425 **Figure 3: Temporal distribution of methane for sites emitting between 10 and 150 mg CH<sub>4</sub> m<sup>-2</sup> d<sup>-1</sup>. (a) Simulated water table position estimated from the soil water content; (b) Simulated (dark line) and observed (gray line) methane emissions released to the atmosphere; (c) Cumulative amount of simulated methane emitted by diffusion, plant mediated transport and ebullition; (d) Methane concentration in the soil layers (dark line) and in the snow layers (gray line) of the model; (e) On the left, depth at which simulated methane production is the highest in the soil, scaled to the maximum peat depth. On the right, the amount of simulated methane produced at these depths.**

430 Sites that emitted between 150 and 400 mgCH<sub>4</sub> m<sup>-2</sup> d<sup>-1</sup> are temperate, sub-arctic and arctic fens (Figure 4).  
 435 Simulated water table positions at FI-Lom, DK-Nuf and PL-Wet are lower in winter than in summer. During the observed period of three years, the simulated water table position at PL-Kpt is lower in summer the first and the last year of observations and higher in summer during the second year. In the winter the methane fluxes are stored in the simulated snow cover at FI-Lom, therefore the simulated surface fluxes above the snow are driven by diffusion. However, during summer simulated methane fluxes essentially originate from plant mediated transport. At DK-Nuf, PL-Kpt and PL-Wet, simulation results show that fewer methane, less than 0.4 gCH<sub>4</sub> m<sup>-2</sup> d<sup>-1</sup>, accumulates in the simulated snow during winter. Methane is transported by vascular plants in summer at DK-Nuf and PL-Wet whereas at PL-Kpt simulated methane fluxes are provided by both vascular plants and ebullition. This is consistent with high soil methane concentrations at PL-Kpt during summer that are near 70 gCH<sub>4</sub> m<sup>-2</sup> the first year and near 90 gCH<sub>4</sub> m<sup>-2</sup> the last two years of observation. In contrast, at FI-Lom simulated soil methane concentrations are near 50 gCH<sub>4</sub> m<sup>-2</sup> during summer whereas the winter concentrations are near 80



440  $\text{gCH}_4 \text{ m}^{-2}$  which is not sufficient to cause methane ebullition. At DK-Nuf and PL-Wet simulated soil methane concentrations  
 are less than  $10 \text{ g CH}_4 \text{ m}^{-2}$  therefore ebullition is not engendered. At FI-Lom, PL-Kpt and PL-Wet, the highest simulated  
 methane production rates are maximum at  $0.3 \text{ g CH}_4 \text{ m}^{-2} \text{ d}^{-1}$  and are steadily near 20cm at PL-Wet and about at 20 cm depth  
 in summer and deepen down to 75 cm depth in winter for the two other sites. While at DK-Nuf the highest simulated  
 methane production rates are lower with values up to  $0.08 \text{ g CH}_4 \text{ m}^{-2} \text{ d}^{-1}$  and take place around 20 cm in the summer and 40  
 445 cm in winter.

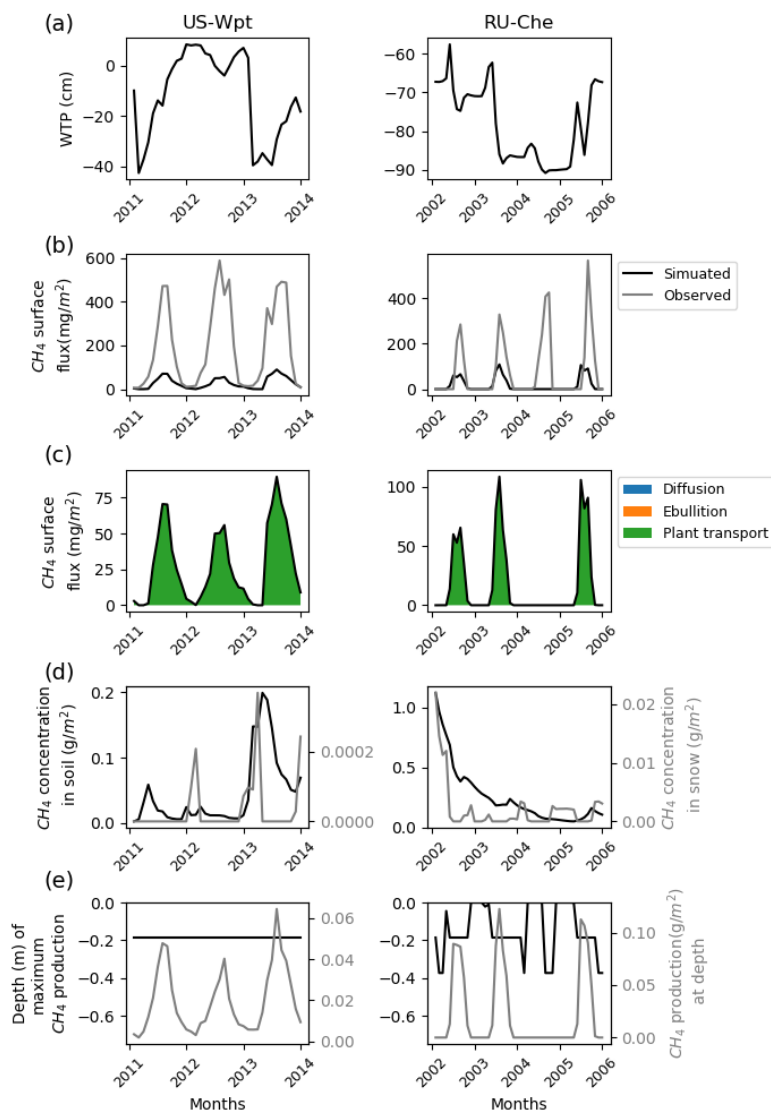


450 **Figure 4: Temporal distribution of methane for sites emitting between  $150$  and  $400 \text{ mg CH}_4 \text{ m}^{-2} \text{ d}^{-1}$ .** (a) Simulated water table  
 position estimated from the soil water content; (b) Simulated (dark line) and observed (gray line) methane emissions released to  
 the atmosphere; (c) Cumulative amount of simulated methane emitted by diffusion, plant mediated transport and ebullition; (d)  
 Methane concentration in the soil layers (dark line) and in the snow layers (gray line) of the model; (e) On the left, depth at which



**simulated methane production is the highest in the soil, scaled to the maximum peat depth. On the right, the amount of simulated methane produced at these depths.**

455           The highest simulated methane fluxes of  $600 \text{ mg CH}_4 \text{ m}^{-2} \text{ d}^{-1}$  were observed at US-Wpt and RU-Che that are  
respectively a temperate marsh and an arctic tundra site. The simulated water table positions at both sites are lower in the  
summer than in the winter and vary for US-Wpt between 10 cm above ground and 40 cm below ground level. At RU-Che  
the prognostic water table depth is very low i.e. 60 to 90cm below the soil surface as for US-Bog. Indeed, both sites are  
underlaid with permafrost which can explain these deeper simulated water table positions. At US-Wpt and RU-Che, site  
460 simulations could only provide methane fluxes up to  $100 \text{ mg CH}_4 \text{ m}^{-2} \text{ d}^{-1}$  despite the expansion of ranges for the optimization  
of the parameters. These simulated fluxes are entirely transported via vascular plant tissues. During the year of highest fluxes  
at both sites, simulated methane concentrations are around  $0.2 \text{ g CH}_4 \text{ m}^{-2}$  of soil however simulated methane concentrations  
in snow are 10 times lower at the marsh site,  $0.3 \text{ mg CH}_4 \text{ m}^{-2}$  than at the tundra site,  $3.0\text{-}4.0 \text{ mg CH}_4 \text{ m}^{-2}$ . At US-Wpt,  
465 simulations show that methane is primarily produced around 20 cm depth at a rate of  $40\text{-}60 \text{ mg CH}_4 \text{ m}^{-2} \text{ d}^{-1}$ . Though, at RU-  
Che, simulated methane production rate is higher around  $100 \text{ mg CH}_4 \text{ m}^{-2} \text{ d}^{-1}$  and occurs at 20 cm depth during summer and  
few centimeters below the surface during winter when snow covers the surface.



470 **Figure 5: Temporal distribution of methane for sites emitting more than 400 mg CH<sub>4</sub> m<sup>-2</sup> d<sup>-1</sup>.** (a) Simulated water table position estimated from the soil water content; (b) Simulated (dark line) and observed (gray line) methane emissions released to the atmosphere; (c) Cumulative amount of simulated methane emitted by diffusion, plant mediated transport and ebullition; (d) Methane concentration in the soil layers (dark line) and in the snow layers (gray line) of the model; (e) On the left, depth at which simulated methane production is the highest in the soil, scaled to the maximum peat depth. On the right, the amount of simulated methane produced at these depths.



### 475 3.2 Multi-site optimization

For large scale simulations only one set of parameters is needed for the simulation of methane emissions to achieve that the average of each parameter value optimized on site are commonly employed. Here, a multi-site optimization has been performed for which prior values correspond to the average values of each parameter obtained from the single site optimizations described in section 3.1. This multi-site optimization serves to assess with which extent a multi-site  
480 optimization is more efficient than using average values of parameters optimized on site independently. Multi-site optimized parameter values acquired by using average values of parameters defined at each site and the initial ranges (Table 3) are shown in Table 5. Compared to the prior values,  $q_{MG}$  stayed about the same, optimized  $k_{MT}$  shifted to values that promote lower oxidation of methane and near the root area the proportion of methane oxidation  $M_{rox}$  is increased. Plant mediated transport rate is stimulated by the increase of  $T_{veg}$  to a value of 9 and the rooting depth is about the same, 0.27 for the prior  
485 and 0.26 for the posterior. Then the capability of methane ebullition in the model is decreased by the increase of the ebullition threshold deriving from  $m_{XRCH_4}$  and the decrease of the probability of bubbles to reach the surface ( $w_{size}$ ).

In Table 7,  $RMSD_{MS\ prior}$  constitutes the difference between observed and simulated emissions resulting from average single site optimized parameters values.  $RMSD_{MS\ post}$  is generated from the multi-site optimization of the parameters. For 7 sites, posterior values of the  $RMSD_{MS}$  are smaller than prior values ( $RMSD_{MS\ prior}$ ) thereby reducing the deviation of  
490 simulated emissions from the observation. The  $RMSD_{MS\ post}$  of the seven other sites are larger than the  $RMSD_{MS\ prior}$ . Among those  $RMSD_{MS}$ , posterior and prior values are very similar by less than one unit for FI-Lom, DK-Nuf, US-Wpt and RU-Che and lower than 16 units at DE-Hmm, PL-Wet and US-Bog.  $NRMSD_{MS}$  values are larger at US-Los, DE-Spw and DE-Sfn where methane emissions are lower. At the other sites, the difference of  $NRMSD_{MS}$  and  $NRMSD_{SS}$  are lower than 1.7 units. These results suggest that for global scale simulations parameters defined by the multi-site optimization should provide  
495 methane emissions estimation with lower uncertainties than when parameters are defined from the average of single site optimization values. Indeed, differences using single site and multi-site optimized parameters, displayed in Figure 6, are of the same order of magnitude for most of sites expect for the three sites that emitted the largest amount of methane, PL-Wet, RU-Che and US-Wpt and the lowest amount of methane, US-Los, DE-Spw and DE-Sfn. However, for those six sites methane emissions differences between observations and simulations is lower when using multi-site optimized parameters.

500 A multi-site optimization has also been performed employing extended ranges of parameter values that are enlarged to the maximum and minimum values obtained for the single site optimizations (Table S3 to S5 and Fig S9). Despite that a different set of parameters were defined (Table S2), discrepancies between observed and simulated emissions (Table S4 and S5 and Fig. S10) are similar to the ones obtained using default parameter ranges.

505



**Table 6. Multi-site prior and optimized values of methane scheme parameters. Parameter prior values are the average value of the parameters optimized at each site. Parameters descriptions and references are in Table3.**

Parameters	Unit	Prior values	Ranges	Posterior values	Uncertainty
q <sub>MG</sub>	[-]	9.28	9.0, 11.0	9.64	0.8
k <sub>MT</sub>	1/d	2.59	1.0, 5.0	3.29	1.6
M <sub>rox</sub>	fraction	0.44	0.0, 1.0	0.70	0.4
Z <sub>root</sub>	m	0.27	0.01, 0.5	0.26	0.196
T <sub>veg</sub>	[-]	6.99	0.0, 15.0	8.62	6.0
wsize	m	0.0088	0.001, 0.1	0.0018	0.396
m <sub>XCH<sub>4</sub></sub>	fraction	0.24	0.05, 0.75	0.57	0.28

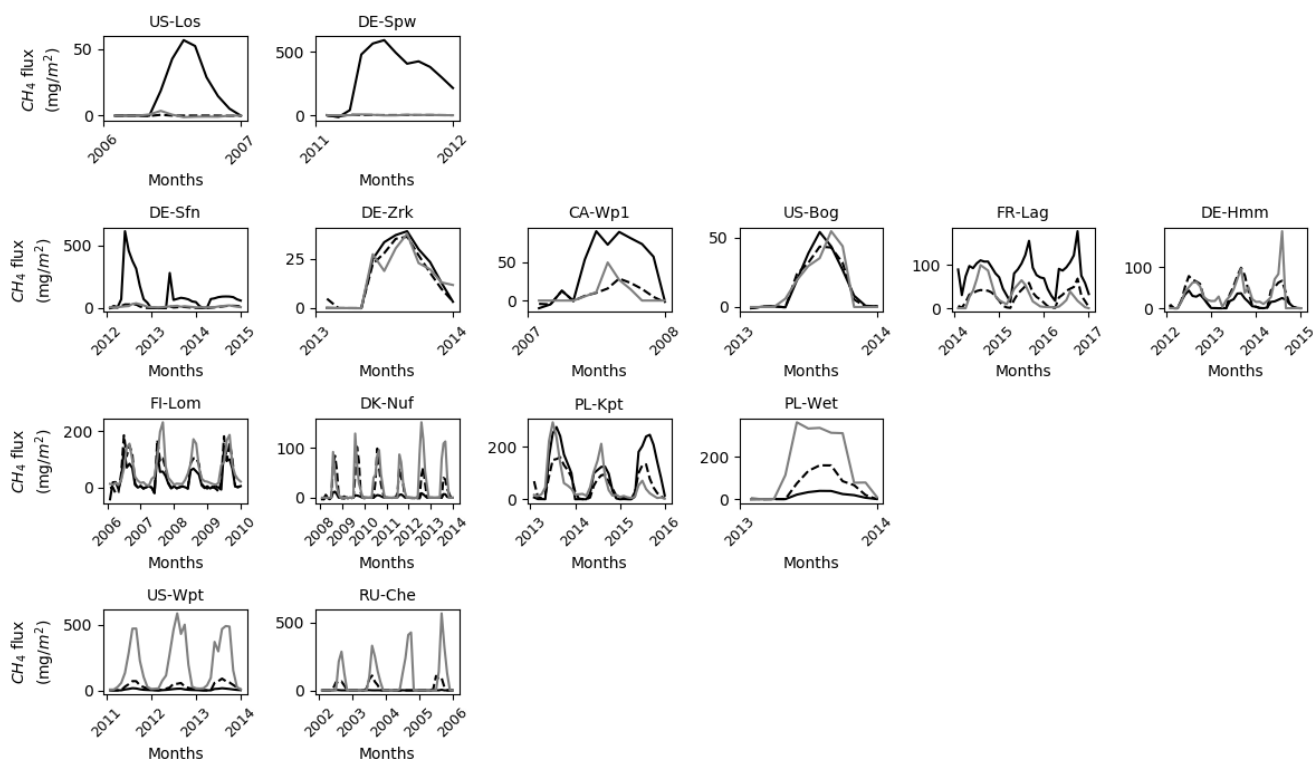
510

**Table 7. Discrepancies between observed and simulated methane emissions are quantified by the root mean square difference (RMSD) approach. Minimization efficiency of the multisite optimization is indicated by the relationship between the prior using average values of parameters optimized by the single site optimization and posterior RMSD<sub>MS</sub> as  $(1 - \text{RMSD}_{\text{MS post}} / \text{RMSD}_{\text{MS prior}}) \times 100$ . Normalized root mean square difference (NRMSD<sub>MS</sub>) is defined by the RMSD<sub>MS</sub> posterior normalized by the annual mean of observed methane emissions of Table 5.**

515

Sites	RMSD <sub>MS</sub> prior	RMSD <sub>MS</sub> posterior	1-(RMSD <sub>MS post</sub> /RMSD <sub>MS prior</sub> )	NRMSD <sub>MS</sub>
US-Los	56.1	24.6	0.56	224.00
DE-spw	855.9	400.1	0.53	800.20
DE-Sfn	325.8	144.6	0.56	37.08
DE-Zrk	26.5	6.6	0.75	1.07
CA-Wpl	91.7	9.0	0.90	1.01
US-Bog	32.2	43.9	-0.36	1.53
FR-Lag	138.7	67.6	0.51	2.51
DE-Hmm	31.8	36.3	-0.14	1.71
FI-Lom	52.2	53.0	-0.01	2.10
DK-NuF	43.9	44.3	-0.01	0.84
PL-Kpt	188.4	78.0	0.59	1.39
PL-Wet	181.1	197.4	-0.09	2.12
US-Wpt	272.2	273.3	-0.004	1.39
RU-Che	159.0	159.4	-0.003	1.98





520 **Figure 6: Simulated and observed (gray line) methane emissions using single site (dashed dark line) and multi-site (solid dark line) optimized parameters.**

## 4. Discussion

### 4.1 Parametrization's sensitivity

525 Sensitivity analyses were previously performed to assess methane emission models responsiveness to parameters values (Meng et al., 2012; Riley et al., 2011; Spahni et al., 2011a; Wania et al., 2009; Zhu et al., 2014). These studies (Van Huissteden et al., 2009; Riley et al., 2011) suggested that temperature dependency of methanogenesis is the most influential parameter affecting methane production whereas methane emissions are mostly sensitive to oxidation and plant transport. Indeed, in large scale models such as CLM4Me, LPJ-GUESS, LPX-Bern, CNRM and ORCHIDEE (Potter, 1997; Riley et al., 2011; Khvorostyanov et al., 2008b; Wania et al., 2009, 2010; Zhu et al., 2014; Morel et al., 2019) methane production  
530 result from anoxic decomposition of soil organic matter which rate is constrained by the soil oxic and anoxic decomposition ratio ( $q_{MG}$ ). Therefore, methanogenesis rate is driven by the same variables as the oxic decomposition that depends on soil temperature and primary production. This ratio was first established from experimental studies that determine the microbial production ratio  $CO_2$  to  $CH_4$  (Potter et al., 1996; Segers, 1998) for various water table positions. These ratio values were



535 found to be between 0.58 and 10000. Because of this wide range of values, process - based models employed this CO<sub>2</sub> to  
CH<sub>4</sub> ratio as an adjustable parameter that is weighted by environmental factors such as soil humidity and temperature. Wania  
et al., (2009) performed a sensitivity analysis study of the LPJ-WHyMe model using 7 sites in which the multi-site  
optimization value of the CO<sub>2</sub>/CH<sub>4</sub> ratio was defined at 10 while other models as CLM4Me use a value of 5. Khvorostyanov  
et al., (2008a) and Morel et al., (2019) used respectively q<sub>MG</sub> values of 9 and 10 to simulate methane emissions from arctic  
peatlands therefore in the present study at first q<sub>MG</sub> were optimized in the range of 9-11 then this range was enlarged only for  
540 sites that underestimate methane emissions. Results show that for 13 sites out of 14, q<sub>MG</sub> values ranging between 8.0 - 10.7  
for the single site optimization approach and using multi-site approach a value of 9.6 were found. As in the previous  
sensitivity analysis studies (Riley et al., 2011) lower q<sub>MG</sub> values were obtained at sites located in the highest latitudes.

After methanogenesis, methane is mobilized in pores and ultimately emitted to the atmosphere or being oxidized by  
methanotrophs depending on whether methane travels along the anoxic or the oxic parts of the soil. In large scale models,  
545 methanotrophy is formulated employing a Michaelis-Mentens or a first order kinetic framework based on soil methane and  
oxygen content (Morel et al., 2019). These formulations are then driven by the oxidation rate which values vary from few  
hours to days. In the present work, we employed the first order kinetic formulation of Khvorostyanov et al., (2008a) that is  
driven by methane and oxygen content. Optimization of the oxidation rate lead to values that are spread over the full range of  
1 to 5 days. This is consistent with the review paper of Smith et al., (2003) that highlight that methanotrophy is more  
550 sensitive to soil humidity than soil temperature and that there is a direct link between methane oxidation rate and gas  
diffusivity. Thus, the optimization of the oxidation rate results from the balance between inputs and outputs that are  
respectively available methane and oxygen substrates and methane fluxes which explain this large variability in oxidation  
rate. In addition, here snow is considered in the diffusion scheme which is in part controlling diffusivity of oxygen from the  
atmosphere to the ground in winter.

555 Methane emissions mediated by vascular plants result from series of processes that include (1) the diffusion and  
advective transport of methane and oxygen in aerenchym tissues (2) autotrophic respiration of a fraction of oxygen transiting  
in aerenchyma of vascular plants (Colmer, 2003; Nielsen et al., 2017) (3) methane production by microbial decomposition of  
plant exudates and (4) methane oxidation by exudates and by remaining oxygen at the root level brought through  
aerenchyma that increase methanotrophs activities. Modelling these processes requires (1) to understand and quantify them  
560 (Kaiser et al., 2017; Raivonen et al., 2017; Riley et al., 2011; Wania, 2007) and (2) to evaluate average density of vascular  
plants that are capable of significant gas transport across ecosystems. While a significant number of studies provide insight  
on gas exchanges through vascular plants, densities of vascular plants with aerenchyma in peatlands is poorly characterized.  
In the most recent models, formulations of various complexity were used to simulate vegetation mediated gas transport  
considering mainly CH<sub>4</sub> and O<sub>2</sub> (Kaiser et al., 2017; Morel et al., 2019; Raivonen et al., 2017; Riley et al., 2011; Wania,  
565 2007). These schemes considered plant transport at the scale of the plant and are based on gas concentration gradients  
between the atmosphere and the soil and some plant traits and properties such as plant height, root diameters, aerenchyma  
porosity and permeability. Because of the biodiversity of peatlands, calibration of parameters accounting for plant traits and



properties of each plant species or family is a cumbersome achievement and the lack of quantification of aerenchymatous plants at the scale of the ecosystem reduces the benefit in considering these characteristics. In the present scheme, vegetation transport of methane is simulated employing the rather simple scheme of Walter and Heimann (2001) that is driven by the rooting depth ( $z_{\text{root}}$ ) of vascular plants with aerenchyma and by the proportion of methane that is oxidized by the rhizosphere ( $M_{\text{rox}}$ ). Optimized  $z_{\text{root}}$  values at sites ranges between 6 and 68 cm depth with the average depth defined at 26 cm which is also the value obtained using the multi-sites approach. These values are consistent with values utilized by Walter and Heimann (2001) that ranged between 0 and 74 cm. It could be expected for  $z_{\text{root}}$  to be set near the depth of maximum methanogenesis as it is the case at DE-Sfn where  $z_{\text{root}}$  is defined at 40 cm. Half of the sites have a  $z_{\text{root}}$  defined between 10 and 60 cm above the depth of maximum methanogenesis and the other remaining values are established between 10 and 50 cm below the depth of maximum methanogenesis. In the rhizosphere methane can also be oxidized at a rate ( $M_{\text{rox}}$ ) that is independent of the rate of methanotrophy. Results of the optimization at site level provided  $M_{\text{rox}}$  values that are scattered over the range of 0 to 1 with the highest values, 0.99, at site, US-Los that emitted the fewest methane and the lowest value, 0.003 at RU-Che that is the site emitted the largest amount of methane. Two trends can be distinguished, for sites that emitted less than  $150 \text{ mg CH}_4 \text{ m}^{-2} \text{ d}^{-1}$  an average of 60% of methane is oxidized by the rhizosphere against 22% at sites emitting more. Across all sites the average proportion of methane oxidized is 44% whereas the optimized value obtained with the multi-site approach is 70%. In previous models, Zhuang et al., (2004) and Wania et al., (2010) employed at the global scale a fixed value of 40 and 50% respectively. With a more realistic and complex formulation in CLM4Me, Riley et al. (2011) estimated that 60% of methane that would have been transferred to the atmosphere by aerenchyma tissues, is instead oxidized by the rhizosphere.  $T_{\text{veg}}$  has been introduced by Walter et al., (1996) to describe the density of plants and their efficiency in methane transport for site estimation. It is an adjustable parameter that was scaled to be between 0 and 15 with lower values for ecosystems dominated by trees and shrubs and the highest values for ecosystems dominated by grasses and sedges. For our 14 sites, optimization at site established  $T_{\text{veg}}$  values between 0.003 and 24 with an average value of 7 and an optimized value at 8.6 for the multi-site approach. Only two values have been defined above 10 at US-Wpt and DK-Nuf which are two sites that are limited in methane substrates which explains these high values of  $T_{\text{veg}}$ .

When methane is significantly produced in the soil, the accumulation of methane in the water saturated pores involves the formation of methane rich bubbles that will migrate in the soil layers and eventually deliver methane to the atmosphere. This flux of methane is commonly prompted in land surface models by the amount of methane that is no longer soluble in saturated water-filled pores. This excess amount is defined here from the mixing ratio ( $m_{\text{rCH}_4}$ ) of methane in bubbles. Then this volumetric content of methane is converted to methane concentration per soil volume in each layer depending on soil temperature and pressure. The optimization of  $m_{\text{rCH}_4}$  at each site leads to values ranging between 3 and 53% with a mean value at 24% whereas the multi-site optimization evaluates  $m_{\text{rCH}_4}$  at 57%. It has been suggested in the literature that the methane partial pressure is sensitive to fluctuations of the hydrostatic and the atmospheric pressure (Tokida et al., 2007b) and of the water table position (Fechner-Levy and Hemond, 1996). Vegetation also impacts the ebullition flux by increasing substrate availability and by stabilizing indefinitely bubbles around roots (Klapstein et al., 2014). Migration of



methane rich-bubbles to the soil surface can be modelled as an instantaneous transport to the atmosphere or to upper layers or by an advective layer-by-layer transport. Here we considered the probability of methane rich-bubble to reach the surface depending on the connectivity between water filled pores (*wsize*). Khvorostyanov et al., (2008a) defined *wsize* at 1cm which establishes a probability of 1 at the surface that decreases to zero at 1.5m depth when soil is saturated. Probability is increasing when *wsize* increases and quickly decreases when soil humidity decreases. In the present study, at each site *wsize* is optimized to values of 0.05 - 3cm. At most sites, optimized *wsize* values are near or below 1cm except for US-Los, DK-Nuf and RU-Che. This might be explained by the low methane concentration in the model soil layers at these sites which annihilate possible emissions by ebullition in the model. The average value across sites corresponds to the same value determined by Khvorostyanov et al., (2008a) at 0.9 cm. A lower value is obtained for the multi-sites optimization of 0.2 cm which reduces occurrence of methane flux by ebullition in our model.

#### 4.2 Methane sources

Soil and litter organic carbon and plant exudates are recognized to be the main substrates for methanogenesis (Chang et al., 2019; Riley et al., 2011; Whalen, 2005). Recent work of Hopple et al., (2019) demonstrates that dissolved organic carbon (DOC) also contributes significantly to anoxic decomposition in peatlands. Some field studies suggested that high latitude methanogenesis can be substrate limited (Chang et al., 2019; Riley et al., 2011; Whalen, 2005). In large scale models, soil organic carbon (SOC) is considered as primary source of methane however in order to increase the rate of methanogenesis labile organic matter such as litter carbon and plant exudates are directly combined to soil carbon bypassing oxic decomposition processes to account them as substrates for the methane production scheme (Morel et al. 2019; Khvonostianov et al; 2008). In the present study, SOC is the only substrate for methanogenesis for which total soil carbon stock and maximum peat depth has been adjusted to observation data at each site (Table 2). Simulation results show that at sites that emitted more than 400mg CH<sub>4</sub> m<sup>-2</sup> d<sup>-1</sup>, US-WPT and RU-Che, methane emissions are lower than expected reflecting the lack of substrate for methanogenesis. Indeed, in land surface models, soil carbon is distributed in three types, the active, the slow and the passive pool. The active pool features labile SOC whereas the slow and the passive pools exert more stable SOC with slower decomposition rates. Integrated SOC accumulated up to 0.75 m by our model for each site is reported in Table 8. These carbon stocks correspond to available substrate for methanogenesis occurring at lower depth than 0.75m depth. The lowest carbon stocks were obtained at US-Los, CA-Wp1, PL-Wet, US-Wpt and RU-Che with a total SOC lower than 50 kg/m<sup>2</sup>. Unlike the other sites, the active SOC contents at US-Wpt and RU-Che are very small respectively 4 and 3.5 kg/m<sup>2</sup> which limit methane production in the model. At both sites, simulated vertical carbon contents were constrained using observed soil bulk density and the carbon accumulation model described in Qiu et al., (2019). Khvorostyanov et al., (2008b) previously performed site simulation at RU-Che in which they prescribed an amount of 15gC m<sup>-2</sup> y<sup>-1</sup> of root exudates that was added to the active SOC leading to emissions up to 300 mg m<sup>-2</sup> d<sup>-1</sup>. As US-Wpt is a marsh it is expected to have a lower total SOC than the other peatland sites. It is also expected that root exudates and DOC in pore



635 water and in above ground reservoirs contribute significantly to methanogenesis which is not explicitly considered in the present version of the model.

**Table 8. Integrated simulated soil organic carbon content of peatland sites up to 0.75 m depth.**

Sites identification	Soil organic carbon content			
	active	slow	passive	total
	kg/m <sup>2</sup>	kg/m <sup>2</sup>	kg/m <sup>2</sup>	kg/m <sup>2</sup>
US-Los	13.94	13.85	0.05	27.84
DE-Spw	33.54	41.09	0.17	74.80
DE-Sfn	28.15	49.40	0.28	77.83
DE-Zrk	44.81	75.92	0.44	121.18
CA-Wpl	12.30	21.75	0.12	34.17
US-Bog	14.16	66.55	0.69	81.40
FR-Lag	33.67	52.02	0.25	85.94
DE-Hmm	27.49	84.08	0.76	112.34
FI-Lom	13.95	63.89	0.85	78.69
DK-NuF	4.18	49.20	1.18	54.56
PL-Kpt	14.19	98.61	1.63	114.44
PL-Wet	15.36	22.08	0.11	37.55
US-Wpt	3.94	0.84	0.001	4.78
RU-Che	3.51	40.04	2.14	45.69

### 4.3 Methane fluxes

640 Sensitivity of methane fluxes to model parameters was evaluated by comparing annual methane emissions obtained by employing SS and MS optimized parameters. Table 9 reports annual observed and simulated methane fluxes and contributions among the three types of methane transport, i.e., diffusion, ebullition and plant mediated. Considering all 14 sites, average annual methane emissions for the observed values is  $18 \pm 18 \text{ g m}^{-2} \text{ y}^{-1}$ , and  $9 \pm 6$  and  $25 \pm 38 \text{ g m}^{-2} \text{ y}^{-1}$  for simulations using respectively SS and MS optimized parameters. Diffusion of methane in the topsoil layers of the model was  
 645 minor compared to other emissions and appeared to act as a sink of methane rather than a source. Plant mediated transport (PMT) were the largest simulated fluxes. For SSO simulations, these PMT fluxes represent between 52 and 74% of the total fluxes at US-Los, DE-Spw, DE-Sfn and PL-Kpt and more than 97% at all the other sites whereas for MSO simulations PMT fluxes are all higher than 98%. Given that diffusion releases little amounts of methane to the atmosphere, remaining fluxes are emitted by ebullition. The largest ebullition fluxes were obtained in SSO simulations whereas fewer methane was  
 650 released by ebullition in MSO simulations. For about half of sites, 3 - 11% of fluxes were furnished via ebullition and less than 1% at the other sites using SSO parameter values. In simulations employing MSO parameters values, ebullition contributed to less than 2% of total fluxes at each site.



Discrepancies between observation data and SSO and MSO simulations are displayed in Figure 6. At sites that emitted the largest amount of methane e.i. PL-Wet, RU-Che and US-Wpt, SSO and MSO simulations were underestimated up to 46 and 53 g CH<sub>4</sub> m<sup>-2</sup> y<sup>-1</sup>, respectively (Fig. S6 to S8). At the other sites when using SSO parameters methane emissions were still underestimated even though this was only about 7 g CH<sub>4</sub> m<sup>-2</sup> y<sup>-1</sup>. While in MSO simulations only three sites, DE-Hmm, FI-Lom and DK-Nuf underestimated methane emissions of 11 g CH<sub>4</sub> m<sup>-2</sup> y<sup>-1</sup> compared to observation data. Simulations that display, in Figure 7, an overestimation of methane emissions were all performed using MSO parameters. At DE-Spw and DE-Sfn methane emissions were overestimated by 118 and 95 g CH<sub>4</sub> m<sup>-2</sup> y<sup>-1</sup>. This large excess of methane emissions results from a significant increase of the parameter Tveg between the SSO and MSO. Indeed, optimized Tveg values at these sites are 0.003 and 0.1 when optimized at site level whereas it was defined at 8.6 with the multi-sites approach. In the model, Tveg established the magnitude of plant mediated fluxes which are constrained by soil methane content, plant growth and root expansion in the soil. This shows that for peatlands where methanogenesis is not substrate limited, Tveg is a key parameter to evaluate methane fluxes. Other sites that display an overestimation of methane emissions using MSO parameters are US-Los, CA-Wp1 and PL-Kpt. For these sites the excess of emissions compared to the observations only extend up to 12 g CH<sub>4</sub> m<sup>-2</sup> y<sup>-1</sup>. Across sites, differences between observed and simulated emissions employing SSO parameters averages around 9 g CH<sub>4</sub> m<sup>-2</sup> y<sup>-1</sup> of methane deficiency. On the contrary, emissions obtained with MSO parameters are in excess of about 5 g CH<sub>4</sub> m<sup>-2</sup> y<sup>-1</sup> on average compared to observations. Average differences between observation and simulation results significantly decreases to -1.2 and 0.5 g CH<sub>4</sub> m<sup>-2</sup> y<sup>-1</sup> for SSO and MSO simulations when excluding sites that emitted more than 300 and less than 20 mg CH<sub>4</sub> m<sup>-2</sup> d<sup>-1</sup>, i.e. PL-Wet, RU-Che and US-Wpt for the SSO simulations and DE-Spw, DE-Sfn, PL-Wet, RU-Che and US-Wpt for the MSO simulations. This shows that the model is better constrained at sites emitting between 20 and 300 mg CH<sub>4</sub> m<sup>-2</sup> d<sup>-1</sup>.

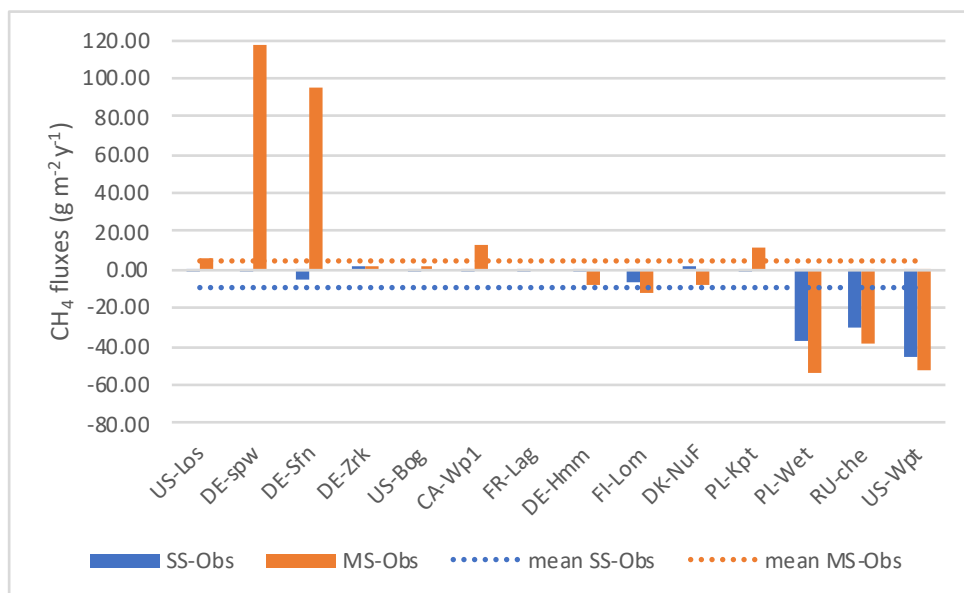
Average methane emissions estimated from these 14 sites can be utilized to roughly calculate emissions from peatlands located northern of 30°N. In Qiu et al. (2019), northern peatlands extent has been estimated using ORCHIDEE\_PEAT v2.0 and compare with three other peatlands inventories and soil data (Batjes, 2016; Joosten, 2009; Xu et al., 2018). All four estimates of northern peatlands areas range between 2823 and 3896 x 10<sup>3</sup> km<sup>2</sup>. Assessments of methane emissions for these northern peatland areas estimated using the average fluxes from measurements yield annual methane fluxes to 51-71 Tg CH<sub>4</sub> y<sup>-1</sup> (Table 9). These annual fluxes are in good agreement with annual methane emissions determined from upscaling of flux measurements of 44-54 Tg CH<sub>4</sub> y<sup>-1</sup> by Zhu et al. (2013). Estimates of annual methane fluxes obtained from the SSO and MSO simulations lead to values of 25 - 35 and 70 - 96 Tg CH<sub>4</sub> y<sup>-1</sup>, respectively. Estimates from SSO simulations are consistent with annual methane emissions reckon from inversion models (Bruhwiler et al., 2014; Spahni et al., 2011b) and other process-based models (Chen et al., 2015; Peltola et al., 2019; Treat et al., n.d.; Zhang et al., 2016). While annual methane emissions assessed from MSO simulations are above the upper range of annual methane fluxes provided by the global methane budget for natural wetlands located northern of 30°N of 12-61 Tg CH<sub>4</sub> y<sup>-1</sup> for bottom-up approach and 31-64 Tg CH<sub>4</sub> y<sup>-1</sup> for top-down approach.



690

**Table 9. Yearly methane emissions defined from the observed data (Obs), from simulations employing optimized parameters obtained by the single site optimization (SSO) and by multi-site optimization (MSO). Methane fluxes combine methane emitted by diffusion, plant mediated transport and ebullition.**

Site	Data	CH <sub>4</sub> fluxes g m <sup>-2</sup> y <sup>-1</sup>	Diffusion g m <sup>-2</sup> y <sup>-1</sup>	Plant mediated transport g m <sup>-2</sup> y <sup>-1</sup>	Ebullition g m <sup>-2</sup> y <sup>-1</sup>
US-Los	Obs	0.05			
	SSO	0.01	0.0031	0.01	0.0
	MSO	6.70	-0.01	6.71	0.0
DE-spw	Obs	0.46			
	SSO	0.07	-0.29	0.34	0.02
	MSO	118.23	-0.48	117.54	1.17
DE-Sfn	Obs	14.01			
	SSO	9.63	-0.22	5.03	4.82
	MSO	108.65	-0.20	106.47	2.38
DE-Zrk	Obs	5.60			
	SSO	5.68	-0.0013	5.53	0.15
	MSO	6.27	-0.0013	6.27	0.01
US-Bog	Obs	5.74			
	SSO	5.48	0.047	5.44	0.0
	MSO	5.85	0.050	5.80	0.0
CA-Wpl	Obs	3.29			
	SSO	3.19	-0.12	3.12	0.19
	MSO	15.63	-0.10	15.72	0.0
FR-Lag	Obs	9.91			
	SSO	9.57	-0.006	9.58	0.0
	MSO	9.91	29.68	0.0	29.68
DE-Hmm	Obs	12.19			
	SSO	10.77	-0.002	10.68	0.09
	MSO	5.03	0.0	4.97	0.06
FI-Lom	Obs	21.15			
	SSO	14.48	-0.23	14.60	0.11
	MSO	9.58	0.040	9.54	0.0
DK-NuF	Obs	8.69			
	SSO	9.42	-0.05	9.21	0.26
	MSO	0.54	0.01	0.54	0.0
PL-Kpt	Obs	21.22			
	SSO	20.35	-0.03	13.78	6.61
	MSO	33.21	-0.03	33.16	0.08
PL-Wet	Obs	58.96			
	SSO	21.31	-0.04	21.25	0.10
	MSO	5.52	-0.005	5.53	0.0
RU-che	Obs	38.92			
	SSO	8.46	-0.0001	8.46	0.0
	MSO	0.16	-0.0007	0.16	0.0
US-Wpt	Obs	53.40			
	SSO	7.61	0.0	7.61	0.0
	MSO	1.55	0.0	1.55	0.0



695 **Figure 7: Differences in annual methane emissions defined between the observed data (Obs), and simulations employing parameters optimized by the single site (SS) and by multi-site (MS) approaches.**

## 5. Conclusion

700 The methane model developed by Khvorostyanov et al., (2008a) has been modified to encompass northern peatlands and permafrost features embedded in the most recent version of ORCHIDEE-PEAT v2.0. This modified version, ORCHIDEE-PCH4 which was used in this study, integrates a vertical discretization of oxic and anoxic decomposition of soil organic carbon of northern peatlands and subsequent methane production, oxidation and transport by vascular plants, ebullition and diffusion in soil and snow layers. A sensitivity analysis of methane emissions was performed on changes of 7 model parameters optimized with site-level measurements of 14 sites located northern than 41°N on the Eurasian and  
705 American continents. ORCHIDEE data assimilation system (Bastrikov et al., 2018) with a genetic algorithm for random search approach have been successfully employed to optimize these 7 parameters at each site and consider methane emissions from all sites simultaneously.

710 Single site optimization results highlighted that the depth of the highest methane production fluctuates between 20 cm during warmer season and 75 cm during the cold season. This demonstrates the sensitivity of methanogenesis to soil temperature and provides insight on the extent to which methanogenesis takes place in the soil layers. This also serves in identifying sites that are substrate limited and to emphasize the need in global scale models to consider explicitly dissolved organic matter as a source of methane substrate. Indeed, in some site simulation studies prescribed methane substrate originating from litter decomposition or plant exudates were directly added to soil organic content in order to balance out the





715 lack of labile substrate. In the scheme of ORCHIDEE-PCH4, the addition of methane diffusion in snow layers during winter exposes the potential of snow to delay methane emissions coming from the soil.

720 Optimization of parameters employing simultaneously methane emissions from all 14 sites engenders a reduction in the rate of methanotrophy and in methane transport in the soil by ebullition promoting methane oxidation at the root level and transport of methane by vascular plants. These involve a large overestimation of sites emitting small amounts of methane. Nonetheless, on average methane emissions simulated employing the multi-site optimization approach are only  
725 overestimated by about  $5 \text{ g CH}_4 \text{ m}^{-2} \text{ y}^{-1}$  because the overestimation of low emitting sites is counterbalanced by high emitting sites that are limited in methane substrates. In contrast, average methane emission obtained using parameters from the single site optimization is underestimated by  $9 \text{ g CH}_4 \text{ m}^{-2} \text{ y}^{-1}$  compared to the average observed fluxes. Nevertheless, extrapolation of this average methane emissions to northern peatland areas reveals that emissions estimated from the multi-site simulation are much larger than emissions estimated from other peatland process-based models and inventories whereas emissions  
730 calculated from the single site optimizations are in good agreement with other estimates. This demonstrates the complexity of interactions of the methane cycle with environmental conditions considered at various scales and the need for more detailed on-site studies.

#### Code availability

735 The source code (doi: 10.14768/d385219a-787a-439c-b128-2e2d30a21f87 ) is available online via [https://forge.ipsl.jussieu.fr/orchidee/wiki/GroupActivities/CodeAvalaibilityPublication/ORCHIDEE\\_mict\\_peat\\_ch4](https://forge.ipsl.jussieu.fr/orchidee/wiki/GroupActivities/CodeAvalaibilityPublication/ORCHIDEE_mict_peat_ch4). Readers interested in running the model should follow the guideline at <http://orchidee.ipsl.fr/index.php/you-orchidee>. The optimization tool is available through a dedicated web site for data assimilation with ORCHIDEE (<https://orchidas.lsce.ipsl.fr>)

735

#### Author contributions

ES revised and modified the implementation of the methane module in ORCHIDEE-PEAT, performed model optimization simulations in ORCHIDEE-PCH4 employing ORCHIDEE data assimilation system, investigated simulation results and prepared the manuscript with contributions from all co-authors. FJ, BG, CG, PC, SG, FL-D conceptualized, secured funding  
740 and supervised the project. CQ, DZ, BG provided ORCHIDEE-PEAT and assisted with model set up and development. LJ, FJ, BG assisted in implementing ORCHIDEE-PCH4 and investigating simulation results. VB, PP provided the model and the expertise on the ORCHIDEE data assimilation system and contributed to the interpretation of simulation results. CG, SG, FL-D, MA, MSB-H, JC, BHC, HC, CWE, ESE, LBF, KF, DH, JK, OK, NK, LK, AL, LM, WP, TS, KZ produced and provided quality field dataset employed to constrain and validate ORCHIDEE-PEAT and ORCHIDEE-PCH4.

745



## Acknowledgments

The modelling work was supported by the European Union's Horizon 2020, Project CRESCENDO under contract 641816 and Labex VOLTAIRE ANR-10-LABX-100-01. The authors acknowledge support of staff at each site. Research at US-Los was supported by the Ameriflux Network Management Project contract #7544821 to the ChEAS core site cluster. Funding  
750 for the measurements in Biebrza National Park was provided by the Polish National Science Centre under projects: UMO-2015/17/B/ST10/02187 and UMO-2020/37/B/ST10/01219. US-Bog was support by the United State National Science Foundation: NSF OPP 1107892, 1503912, 1936712. L.B. Flanagan acknowledges funding from the Natural Sciences and Engineering Research Council of Canada (NSERC), the FLUXNET-Canada Network (NSERC, the Canadian Foundation for  
755 Climate and Atmospheric Sciences (CFCAS), and BIOCAP Canada), and the Canadian Carbon Program (CFCAS). Field work at FR-Lag was funded as part of the Labex VOLTAIRE and the PIVOTS project of the Région Centre –Val de Loire (ARD 2020 program and CPER 2015–2020) in the framework of the French Peatland Observatory, SNO Tourbières, endorsed by CNRS-INSU. Research work at DE-Hmm was funded by the Deutsche Forschungsgemeinschaft under Germany's Excellence Strategy – EXC 177 'CliSAP - Integrated Climate System Analysis and Prediction' – contributing to the Center for Earth System Research and Sustainability (CEN) of Universität Hamburg. The work at PL-Wet is based on  
760 use of Large Research Infrastructure CzeCOS supported by the Ministry of Education, Youth and Sports of CR within the CzeCOS program, grant number LM2018123. N. K. acknowledges the support by SustES – Adaptation strategies for sustainable ecosystem services and food security under adverse environmental conditions (CZ.02.1.01/0.0/0.0/16\_019/0000797).

765

## References

- Allan, W., Struthers, H. and Lowe, D. C.: Methane carbon isotope effects caused by atomic chlorine in the marine boundary layer: Global model results compared with Southern Hemisphere measurements, *J. Geophys. Res. Atmos.*,  
770 doi:10.1029/2006JD007369, 2007.
- Anav, A., Friedlingstein, P., Kidston, M., Bopp, L., Ciais, P., Cox, P., Jones, C., Jung, M., Myneni, R. and Zhu, Z.: Evaluating the land and ocean components of the global carbon cycle in the CMIP5 earth system models, *J. Clim.*, doi:10.1175/JCLI-D-12-00417.1, 2013.
- Bastrikov, V., MacBean, N., Bacour, C., Santaren, D., Kuppel, S. and Peylin, P.: Land surface model parameter optimisation using in situ flux data: comparison of gradient-based versus random search algorithms (a case study using ORCHIDEE v1.9.5.2), *Geosci. Model Dev.*, 11(12), 4739–4754, doi:10.5194/gmd-11-4739-2018, 2018.
- Batjes, N. H.: Harmonized soil property values for broad-scale modelling (WISE30sec) with estimates of global soil carbon



- stocks, *Geoderma*, 269, 61–68, doi:10.1016/J.GEODERMA.2016.01.034, 2016.
- 780 Blake, D. R., Mayer, E. W., Tyler, S. C., Makide, Y., Montague, D. C. and Rowland, F. S.: Global increase in atmospheric methane concentrations between 1978 and 1980, *Geophys. Res. Lett.*, doi:10.1029/GL009i004p00477, 1982.
- Blodau, C.: Carbon cycling in peatlands - A review of processes and controls, *Environ. Rev.*, 10(2), 111–134, doi:10.1139/a02-004, 2002.
- Bridgman, S. D., Cadillo-Quiroz, H., Keller, J. K. and Zhuang, Q.: Methane emissions from wetlands: Biogeochemical, microbial, and modeling perspectives from local to global scales, *Glob. Chang. Biol.*, 19(5), 1325–1346, doi:10.1111/gcb.12131, 2013.
- 785 Bruhwiler, L., Dlugokencky, E., Masarie, K., Ishizawa, M., Andrews, A., Miller, J., Sweeney, C., Tans, P. and Worthy, D.: CarbonTracker-CH<sub>4</sub>: an assimilation system for estimating emissions of atmospheric methane, *Atmos. Chem. Phys.*, 14, 8269–8293, doi:10.5194/acp-14-8269-2014, 2014.
- Chang, K. Y., Riley, W. J., Brodie, E. L., McCalley, C. K., Crill, P. M. and Grant, R. F.: Methane Production Pathway Regulated Proximally by Substrate Availability and Distally by Temperature in a High-Latitude Mire Complex, *J. Geophys. Res. Biogeosciences*, doi:10.1029/2019JG005355, 2019.
- 790 Chanton, J. P. and Whiting, G. J.: Trace gas exchange in freshwater and coastal marine environments: ebullition and transport by plants., in *Biogenic trace gases: measuring emissions from soil and water*, edited by R. (eds) Matson, PA, Harriss, Blackwell, Oxford., 1995.
- 795 Chen, X., Bohn, T. J. and Lettenmaier, D. P.: Model estimates of climate controls on pan-Arctic wetland methane emissions, *Biogeosciences*, 12, 6259–6277, doi:10.5194/bg-12-6259-2015, 2015.
- Colmer, T. D.: Long-distance transport of gases in plants: A perspective on internal aeration and radial oxygen loss from roots, *Plant, Cell Environ.*, doi:10.1046/j.1365-3040.2003.00846.x, 2003.
- Dlugokencky, E.: Trends in Atmospheric Methane, *Earth Syst. Res. Lab.*, 2019.
- 800 Duval, B. and Goodwin, S.: Methane production and release from two New England peatlands, *Int. Microbiol.*, 3(2), 89–96, doi:10.1007/s00248-005-0264-2, 2000.
- Etheridge, D. M., Steele, L. P., Francey, R. J. and Langenfelds, R. L.: Atmospheric methane between 1000 A.D. and present: Evidence of anthropogenic emissions and climatic variability, *J. Geophys. Res. Atmos.*, doi:10.1029/98JD00923, 1998.
- Etminan, M., Myhre, G., Highwood, E. J. and Shine, K. P.: Radiative forcing of carbon dioxide, methane, and nitrous oxide: A significant revision of the methane radiative forcing, *Geophys. Res. Lett.*, doi:10.1002/2016GL071930, 2016.
- 805 Fechner-Levy, E. J. and Hemond, H. F.: Trapped methane volume and potential effects on methane ebullition in a northern peatland, *Limnol. Oceanogr.*, doi:10.4319/lo.1996.41.7.1375, 1996.
- Goldberg, D.: Genetic algorithms in search, optimization, and machine learning, *Addison wesley*, 102(36), doi:10.5860/choice.27-0936, 1989.
- 810 Gorham, E.: Northern peatlands: role in the carbon cycle and probable responses to climatic warming, *Ecol. Appl.*, 1(2), 182–195, doi:10.2307/1941811, 1991.



- Guimberteau, M., Zhu, D., Maignan, F., Huang, Y., Yue, C., Dantec-N d lec, S., Ottl, C., Jornet-Puig, A., Bastos, A.,  
Laurent, P., Goll, D., Bowring, S., Chang, J., Guenet, B., Tifafi, M., Peng, S., Krinner, G., Ducharne, A. s., Wang, F., Wang,  
T., Wang, X., Wang, Y., Yin, Z., Lauerwald, R., Joetzer, E., Qiu, C., Kim, H. and Ciais, P.: ORCHIDEE-MICT (v8.4.1), a  
815 land surface model for the high latitudes: model description and validation, *Geosci. Model Dev.*, 11(1), 121–163,  
doi:10.5194/gmd-11-121-2018, 2018.
- Haupt, R. L. and Haupt, S. E.: *Practical Genetic Algorithms.*, 2004.
- Hillel, D.: *Introduction to soil physics* New York, Academic Press, 1982.
- Hodgman, C. D.: Hodgman, Charles D. *Handbook of chemistry and physics.* Cleveland, Ohio (2310 Superior Avenue N.  
820 E.): Chemical Rubber Publishing Company, 1954. 3173 P. \$8.50, , doi:10.1002/sce.3730390390, 1960.
- Hopple, A. M., Pfeifer-Meister, L., Zalman, C. A., Keller, J. K., Tfiaily, M. M., Wilson, R. M., Chanton, J. P. and Bridgham,  
S. D.: Does dissolved organic matter or solid peat fuel anaerobic respiration in peatlands?, ,  
doi:10.1016/j.geoderma.2019.04.040, 2019.
- Van Huissteden, J., Petrescu, A. M. R., Hendriks, D. M. D. and Rebel, K. T.: Sensitivity analysis of a wetland methane  
825 emission model based on temperate and arctic wetland sites ments of wetland CH 4 modelling will result from improve-ment  
of wetland vegetation data. [online] Available from: [www.biogeosciences.net/6/3035/2009/](http://www.biogeosciences.net/6/3035/2009/) (Accessed 15 March 2021),  
2009.
- Joosten, H.: *The Global Peatland CO2 Picture: peatland status and drainage related emissions in all countries of the world.*,  
Glob. Peatl. CO2 Pict. Peatl. status Drain. Relat. Emiss. all Ctries. world., 2009.
- 830 Kaiser, S., Göckede, M., Castro-Morales, K., Knoblauch, C., Ekici, A., Kleinen, T., Zubrzycki, S., Sachs, T., Wille, C. and  
Beer, C.: Process-based modelling of the methane balance in periglacial landscapes (JSBACH-methane), *Geosci. Model  
Dev.*, doi:10.5194/gmd-10-333-2017, 2017.
- Khvorostyanov, D. V., Krinner, G., Ciais, P., Heimann, M. and Zimov, S. A.: Vulnerability of permafrost carbon to global  
warming. Part I: Model description and role of heat generated by organic matter decomposition, *Tellus, Ser. B Chem. Phys.*  
835 *Meteorol.*, 60 B(2), 250–264, doi:10.1111/j.1600-0889.2007.00333.x, 2008a.
- Khvorostyanov, D. V., Ciais, P., Krinner, G., Zimov, S. A., Corradi, C. and Guggenberger, G.: Vulnerability of permafrost  
carbon to global warming. Part II: Sensitivity of permafrost carbon stock to global warming, *Tellus, Ser. B Chem. Phys.*  
*Meteorol.*, 60 B(2), 265–275, doi:10.1111/j.1600-0889.2007.00336.x, 2008b.
- Kirschke, S., Bousquet, P., Ciais, P., Saunois, M., Canadell, J. G., Dlugokencky, E. J., Bergamaschi, P., Bergmann, D.,  
840 Blake, D. R., Bruhwiler, L., Cameron-Smith, P., Castaldi, S., Chevallier, F., Feng, L., Fraser, A., Heimann, M., Hodson, E.  
L., Houweling, S., Josse, B., Fraser, P. J., Krummel, P. B., Lamarque, J. F., Langenfelds, R. L., Le Quéré, C., Naik, V.,  
O’doherty, S., Palmer, P. I., Pison, I., Plummer, D., Poulter, B., Prinn, R. G., Rigby, M., Ringeval, B., Santini, M., Schmidt,  
M., Shindell, D. T., Simpson, I. J., Spahni, R., Steele, L. P., Strode, S. A., Sudo, K., Szopa, S., Van Der Werf, G. R.,  
Voulgarakis, A., Van Weele, M., Weiss, R. F., Williams, J. E. and Zeng, G.: Three decades of global methane sources and  
845 sinks, *Nat. Geosci.*, 6(10), 813–823, doi:10.1038/ngeo1955, 2013.



- Klapstein, S. J., Turetsky, M. R., McGuire, A. D., Harden, J. W., Czimeczik, C. I., Xu, X., Chanton, J. P. and Waddington, J. M.: Controls on methane released through ebullition in peatlands affected by permafrost degradation, *J. Geophys. Res. Biogeosciences*, doi:10.1002/2013JG002441, 2014.
- 850 Krüger, M., Eller, G., Conrad, R. and Frenzel, P.: Seasonal variation in pathways of CH<sub>4</sub> production and in CH<sub>4</sub> oxidation in rice fields determined by stable carbon isotopes and specific inhibitors, *Glob. Chang. Biol.*, doi:10.1046/j.1365-2486.2002.00476.x, 2002.
- Largeron, C., Krinner, G., Ciais, P. and Brutel-Vuilmet, C.: Implementing northern peatlands in a global land surface model: Description and evaluation in the ORCHIDEE high-latitude version model (ORC-HL-PEAT), *Geosci. Model Dev.*, 11(8), 3279–3297, doi:10.5194/gmd-11-3279-2018, 2018.
- 855 Meng, L., Hess, P. G. M., Mahowald, N. M., Yavitt, J. B., Riley, W. J., Subin, Z. M., Lawrence, D. M., Swenson, S. C., Jauhainen, J. and Fuka, D. R.: Sensitivity of wetland methane emissions to model assumptions: application and model testing against site observations, *Biogeosciences*, 9, 2793–2819, doi:10.5194/bg-9-2793-2012, 2012.
- Le Mer, J. and Roger, P.: Production, oxidation, emission and consumption of methane by soils: A review, *Eur. J. Soil Biol.*, 37(1), 25–50, doi:10.1016/S1164-5563(01)01067-6, 2001.
- 860 Morel, X., Decharme, B., Delire, C., Krinner, G., Lund, M., Hansen, B. U. and Mastepanov, M.: A New Process-Based Soil Methane Scheme: Evaluation Over Arctic Field Sites With the ISBA Land Surface Model, *J. Adv. Model. Earth Syst.*, 11(1), 293–326, doi:10.1029/2018MS001329, 2019.
- Nielsen, C. S., Michelsen, A., Ambus, P., Deepagoda, T. K. K. C. and Elberling, B.: Linking rhizospheric CH<sub>4</sub>oxidation and net CH<sub>4</sub>emissions in an arctic wetland based on <sup>13</sup>CH<sub>4</sub>labeling of mesocosms, *Plant Soil*, doi:10.1007/s11104-016-3061-4, 865 2017.
- Parton, W. J., Stewart, J. W. B. and Cole, C. V.: Dynamics of C, N, P and S in grassland soils: a model, *Biogeochemistry*, 5(1), 109–131, doi:10.1007/BF02180320, 1988.
- Peltola, O., Vesala, T., Gao, Y., Rätty, O., Alekseychik, P., Aurela, M., Chojnicki, B., Desai, A. R., Dolman, A. J., Euskirchen, E. S., Friborg, T., Göckede, M., Helbig, M., Humphreys, E., Jackson, R. B., Jocher, G., Joos, F., Klatt, J., Knox, 870 S. H., Kowalska, N., Kutzbach, L., Lienert, S., Lohila, A., Mammarella, I., Nadeau, D. F., Nilsson, M. B., Oechel, W. C., Peichl, M., Pypker, T., Quinton, W., Rinne, J., Sachs, T., Samson, M., Schmid, H. P., Sonntag, O., Wille, C., Zona, D. and Aalto, T.: Monthly gridded data product of northern wetland methane emissions based on upscaling eddy covariance observations, *Earth Syst. Sci. Data*, 11(3), 1263–1289, doi:10.5194/essd-11-1263-2019, 2019.
- Potter, C. S.: An ecosystem simulation model for methane production and emission from wetlands, *Global Biogeochem. Cycles*, 11(4), 495–506, doi:10.1029/97GB02302, 1997.
- 875 Potter, C. S., Davidson, E. A. and Verchot, L. V.: Estimation of global biogeochemical controls and seasonality in soil methane consumption, *Chemosphere*, doi:10.1016/0045-6535(96)00119-1, 1996.
- Prather, M., Derwent, R., Ehhalt, D., Fraser, P., Sanhueza, E. and Zhou, X.: Other trace gases and atmospheric chemistry, in *Climate Change 1994: Radiative Forcing of Climate Change and an Evaluation of the IPCC IS92 Emission Scenarios*, edited



- 880 by J. T. Houghton, L. G. Meira Filho, J. Bruce, H. Lee, B. A. Callander, E. Haites, N. Harris, and K. Maskell, pp. 73–126.,  
1995.
- Prather, M. J., Holmes, C. D. and Hsu, J.: Reactive greenhouse gas scenarios: Systematic exploration of uncertainties and the  
role of atmospheric chemistry, *Geophys. Res. Lett.*, doi:10.1029/2012GL051440, 2012.
- Press, W. H., Teukolsky, S. A., Vetterling, W. T. and Flannery, B. P.: *Numerical Recipes in Fortran 77: the art of scientific*  
885 *computing*, in *Numerical Recipes in Fortran 77.*, 1997.
- Prinn, R. G., Weiss, R. F., Arduini, J., Arnold, T., Langley Dewitt, H., Fraser, P. J., Ganesan, A. L., Gasore, J., Harth, C. M.,  
Hermansen, O., Kim, J., Krummel, P. B., Li, S., Loh, Z. M., Lunder, C. R., Maione, M., Manning, A. J., Miller, B. R.,  
Mitrevski, B., Mühle, J., O’Doherty, S., Park, S., Reimann, S., Rigby, M., Saito, T., Salameh, P. K., Schmidt, R., Simmonds,  
P. G., Paul Steele, L., Vollmer, M. K., Wang, R. H., Yao, B., Yokouchi, Y., Young, D. and Zhou, L.: History of chemically  
890 and radiatively important atmospheric gases from the Advanced Global Atmospheric Gases Experiment (AGAGE), *Earth*  
*Syst. Sci. Data*, doi:10.5194/essd-10-985-2018, 2018.
- Qiu, C., Zhu, D., Ciais, P., Guenet, B., Krinner, G., Peng, S., Aurela, M., Bernhofer, C., Brümmner, C., Bret-Harte, S., Chu,  
H., Chen, J., Desai, A. R., Dušek, J., Euskirchen, E. S., Fortuniak, K., Flanagan, L. B., Friborg, T., Grygoruk, M., Gogo, S.,  
Grünwald, T., Hansen, B. U., Holl, D., Humphreys, E., Hurkuck, M., Kiely, G., Klatt, J., Kutzbach, L., Langeron, C.,  
895 Laggoun-Défarge, F., Lund, M., Lafleur, P. M., Li, X., Mammarella, I., Merbold, L., Nilsson, M. B., Olejnik, J., Ottosson-  
Löfvenius, M., Oechel, W., Parmentier, F. J. W., Peichl, M., Pirk, N., Peltola, O., Pawlak, W., Rasse, D., Rinne, J., Shaver,  
G., Peter Schmid, H., Sottocornola, M., Steinbrecher, R., Sachs, T., Urbaniak, M., Zona, D. and Ziemblinska, K.:  
ORCHIDEE-PEAT (revision 4596), a model for northern peatland CO<sub>2</sub>, water, and energy fluxes on daily to annual scales,  
*Geosci. Model Dev.*, 11(2), 497–519, doi:10.5194/gmd-11-497-2018, 2018.
- 900 Qiu, C., Zhu, D., Ciais, P., Guenet, B., Peng, S., Krinner, G., Tootchi, A., Ducharne, A. and Hastie, A.: Modelling northern  
peatland area and carbon dynamics since the Holocene with the ORCHIDEE-PEAT land surface model (SVN r5488),  
*Geosci. Model Dev.*, 12(7), 2961–2982, doi:10.5194/gmd-12-2961-2019, 2019.
- Raivonen, M., Smolander, S., Backman, L., Susiluoto, J., Aalto, T., Markkanen, T., Mäkelä, J., Rinne, J., Peltola, O., Aurela,  
M., Lohila, A., Tomasic, M., Li, X., Larmola, T., Juutinen, S., Tuittila, E. S., Heimann, M., Sevanto, S., Kleinen, T.,  
905 Brovkin, V. and Vesala, T.: HIMMELI v1.0: Helsinki Model of Methane build-up and emission for peatlands, *Geosci.*  
*Model Dev.*, doi:10.5194/gmd-10-4665-2017, 2017.
- Raynaud, D., Blunier, T., Ono, Y. and Delmas, R. J.: *The Late Quaternary History of Atmospheric Trace Gases and*  
*Aerosols: Interactions Between Climate and Biogeochemical Cycles.*, 2003.
- Riley, W. J., Subin, Z. M., Lawrence, D. M., Swenson, S. C., Torn, M. S., Meng, L., Mahowald, N. M. and Hess, P.: Barriers  
910 to predicting changes in global terrestrial methane fluxes: Analyses using CLM4Me, a methane biogeochemistry model  
integrated in CESM, *Biogeosciences*, 8(7), 1925–1953, doi:10.5194/bg-8-1925-2011, 2011.
- Saunio, M., Bousquet, P., Poulter, B., Peregón, A., Ciais, P., Canadell, J. G., Dlugokencky, E. J., Etiope, G., Bastviken, D.,  
Houweling, S., Janssens-Maenhout, G., Tubiello, F. N., Castaldi, S., Jackson, R. B., Alexe, M., Arora, V. K., Beerling, D. J.,



- 915 Bergamaschi, P., Blake, D. R., Brailsford, G., Brovkin, V., Bruhwiler, L., Crevoisier, C., Crill, P., Covey, K., Curry, C.,  
Frankenberg, C., Gedney, N., Höglund-Isaksson, L., Ishizawa, M., Ito, A., Joos, F., Kim, H. S., Kleinen, T., Krummel, P.,  
Lamarque, J. F., Langenfelds, R., Locatelli, R., Machida, T., Maksyutov, S., McDonald, K. C., Marshall, J., Melton, J. R.,  
Morino, I., Naik, V., O'Doherty, S., Parmentier, F. J. W., Patra, P. K., Peng, C., Peng, S., Peters, G. P., Pison, I., Prigent, C.,  
Prinn, R., Ramonet, M., Riley, W. J., Saito, M., Santini, M., Schroeder, R., Simpson, I. J., Spahni, R., Steele, P., Takizawa,  
A., Thornton, B. F., Tian, H., Tohjima, Y., Viovy, N., Voulgarakis, A., Van Weele, M., Van Der Werf, G. R., Weiss, R.,  
920 Wiedinmyer, C., Wilton, D. J., Wiltshire, A., Worthy, D., Wunch, D., Xu, X., Yoshida, Y., Zhang, B., Zhang, Z. and Zhu,  
Q.: The global methane budget 2000-2012, *Earth Syst. Sci. Data*, 8(2), 697–751, doi:10.5194/essd-8-697-2016, 2016.
- Saunio, M., R. Stavert, A., Poulter, B., Bousquet, P., G. Canadell, J., B. Jackson, R., A. Raymond, P., J. Dlugokencky, E.,  
Houweling, S., K. Patra, P., Ciais, P., K. Arora, V., Bastviken, D., Bergamaschi, P., R. Blake, D., Brailsford, G., Bruhwiler,  
L., M. Carlson, K., Carrol, M., Castaldi, S., Chandra, N., Crevoisier, C., M. Crill, P., Covey, K., L. Curry, C., Etiope, G.,  
925 Frankenberg, C., Gedney, N., I. Hegglin, M., Höglund-Isaksson, L., Hugelius, G., Ishizawa, M., Ito, A., Janssens-Maenhout,  
G., M. Jensen, K., Joos, F., Kleinen, T., B. Krummel, P., L. Langenfelds, R., G. Laruelle, G., Liu, L., MacHida, T.,  
Maksyutov, S., C. McDonald, K., McNorton, J., A. Miller, P., R. Melton, J., Morino, I., Müller, J., Murguia-Flores, F., Naik,  
V., Niwa, Y., Noce, S., O'Doherty, S., J. Parker, R., Peng, C., Peng, S., P. Peters, G., Prigent, C., Prinn, R., Ramonet, M.,  
Regnier, P., J. Riley, W., A. Rosentreter, J., Segers, A., J. Simpson, I., Shi, H., J. Smith, S., Paul Steele, L., F. Thornton, B.,  
930 Tian, H., Tohjima, Y., N. Tubiello, F., Tsuruta, A., Viovy, N., Voulgarakis, A., S. Weber, T., Van Weele, M., R. Van Der  
Werf, G., F. Weiss, R., Worthy, D., Wunch, D., Yin, Y., Yoshida, Y., Zhang, W., Zhang, Z., Zhao, Y., Zheng, B., Zhu, Q.,  
Zhu, Q. and Zhuang, Q.: The global methane budget 2000-2017, *Earth Syst. Sci. Data*, doi:10.5194/essd-12-1561-2020,  
2020.
- Segers, R.: Methane production and methane consumption: A review of processes underlying wetland methane fluxes,  
935 *Biogeochemistry*, doi:10.1023/A:1005929032764, 1998.
- Smith, K. A., Ball, T., Conen, F., Dobbie, K. E., Massheder, J. and Rey, A.: Exchange of greenhouse gases between soil and  
atmosphere: Interactions of soil physical factors and biological processes, *Eur. J. Soil Sci.*, doi:10.1046/j.1351-  
0754.2003.0567.x, 2003.
- Smith, R. L., Howes, B. L. and Garabedian, S. P.: In situ measurement of methane oxidation in groundwater by using  
940 natural-gradient tracer tests, *Appl. Environ. Microbiol.*, doi:10.1128/aem.57.7.1997-2004.1991, 1991.
- Spahni, R., Wania, R., Neef, L., Van Weele, M., Pison, I., Bousquet, P., Frankenberg, C., Foster, P. N., Joos, F., Prentice, I.  
C. and Van Velthoven, P.: Constraining global methane emissions and uptake by ecosystems, *Biogeosciences*, 8, 1643–1665,  
doi:10.5194/bg-8-1643-2011, 2011a.
- Spahni, R., Wania, R., Neef, L., Van Weele, M., Pison, I., Bousquet, P., Frankenberg, C., Foster, P. N., Joos, F., Prentice, I.  
945 C. and Van Velthoven, P.: Constraining global methane emissions and uptake by ecosystems, *Biogeosciences*, 8, 1643–1665,  
doi:10.5194/bg-8-1643-2011, 2011b.
- Strack, M., Waddington, J. M., Turetsky, M., Roulet, N. T. and Byrne, K. A.: Northern peatlands, greenhouse gas exchange



- and climate change, in *Peatlands and Climate Change.*, 2008.
- Thornton, J. A., Kercher, J. P., Riedel, T. P., Wagner, N. L., Cozic, J., Holloway, J. S., Dubé, W. P., Wolfe, G. M., Quinn, P.  
950 K., Middlebrook, A. M., Alexander, B. and Brown, S. S.: A large atomic chlorine source inferred from mid-continental  
reactive nitrogen chemistry, *Nature*, doi:10.1038/nature08905, 2010.
- Tokida, T., Mizoguchi, M., Miyazaki, T., Kagemoto, A., Nagata, O. and Hatano, R.: Episodic release of methane bubbles  
from peatland during spring thaw, *Chemosphere*, doi:10.1016/j.chemosphere.2007.06.042, 2007a.
- Tokida, T., Miyazaki, T., Mizoguchi, M., Nagata, O., Takakai, F., Kagemoto, A. and Hatano, R.: Falling atmospheric  
955 pressure as a trigger for methane ebullition from peatland, *Global Biogeochem. Cycles*, doi:10.1029/2006GB002790, 2007b.
- Treat, C. C., Bloom, A. A. and Marushchak, M. E.: Non-growing season methane emissions are a significant component of  
annual emissions across northern ecosystems., n.d.
- Walter, B. P., Heimann, M., Shannon, R. D. and White, J. R.: A process-based model to derive methane emissions from  
natural wetlands, *Geophys. Res. Lett.*, 23(25), 3731–3734, doi:10.1029/96GL03577, 1996.
- 960 Walter, P. and Heimann, M.: A process-based, climate-sensitive model to derive methane emissions from natural wetlands:  
Application to five wetland sites, sensitivity to model parameters, and climate, *New York*, 14(3), 745–765, 2000.
- Wang, T., Ottlé, C., Boone, A., Ciais, P., Brun, E., Morin, S., Krinner, G., Piao, S. and Peng, S.: Evaluation of an improved  
intermediate complexity snow scheme in the ORCHIDEE land surface model, *J. Geophys. Res. Atmos.*, 118(12), 6064–  
6079, doi:10.1002/jgrd.50395, 2013.
- 965 Wania, R.: Modelling northern peatland land surface processes, vegetation dynamics and methane emissions, 2007.
- Wania, R., Ross, I. and Prentice, I. C.: Integrating peatlands and permafrost into a dynamic global vegetation model: 1.  
Evaluation and sensitivity of physical land surface processes, *Global Biogeochem. Cycles*, 23(3), n/a-n/a,  
doi:10.1029/2008GB003412, 2009.
- Wania, R., Ross, I. and Prentice, I. C.: Implementation and evaluation of a new methane model within a dynamic global  
970 vegetation model: LPJ-WHyMe v1.3.1, *Geosci. Model Dev.*, 3(2), 565–584, doi:10.5194/gmd-3-565-2010, 2010.
- Whalen, S. C.: Biogeochemistry of methane exchange between natural wetlands and the atmosphere, *Environ. Eng. Sci.*,  
doi:10.1089/ees.2005.22.73, 2005.
- Wiesenburg, D. A. and Guinasso, N. L.: Equilibrium Solubilities of Methane, Carbon Monoxide, and Hydrogen in Water  
and Sea Water, *J. Chem. Eng. Data*, 24(4), 356–360, doi:10.1021/je60083a006, 1979.
- 975 Xu, J., Morris, P. J., Liu, J. and Holden, J.: PEATMAP: Refining estimates of global peatland distribution based on a meta-  
analysis, *Catena*, 160(December 2017), 134–140, doi:10.1016/j.catena.2017.09.010, 2018.
- Xu, X., Yuan, F., Hanson, P. J., Wullschlegel, S. D., Thornton, P. E., Riley, W. J., Song, X., Graham, D. E., Song, C. and  
Tian, H.: Reviews and syntheses: Four decades of modeling methane cycling in terrestrial ecosystems, *Biogeosciences*,  
13(12), 3735–3755, doi:10.5194/bg-13-3735-2016, 2016.
- 980 Zhang, Z., Zimmermann, N. E., Kaplan, J. O. and Poulter, B.: Modeling spatiotemporal dynamics of global wetlands:  
comprehensive evaluation of a new sub-grid TOPMODEL parameterization and uncertainties, *Biogeosciences*, 13, 1387–





1408, doi:10.5194/bg-13-1387-2016, 2016.

Zhu, Q., Liu, J., Peng, C., Chen, H., Fang, X., Jiang, H., Yang, G., Zhu, D., Wang, W. and Zhou, X.: Modelling methane emissions from natural wetlands by development and application of the TRIPLEX-GHG model, *Geosci. Model Dev.*, 7, 981–985, doi:10.5194/gmd-7-981-2014, 2014.

Zhuang, Q., Melillo, J. M., Kicklighter, D. W., Prinn, R. G., McGuire, A. D., Steudler, P. A., Felzer, B. S. and Hu, S.: Methane fluxes between terrestrial ecosystems and the atmosphere at northern high latitudes during the past century: A retrospective analysis with a process-based biogeochemistry model, *Global Biogeochem. Cycles*, 18(3), doi:10.1029/2004GB002239, 2004.

990